Palaeogeography, Palaeoclimatology, Palaeoecology 670 (2025) 112951

Contents lists available at ScienceDirect

Palaeogeography, Palaeoclimatology, Palaeoecology

journal homepage: www.elsevier.com/locate/palaeo

The Cambrian ROECE and DICE carbon isotope excursions in western Gondwana (Montagne Noire, southern France): Implications for regional and global correlations of the Miaolingian Series

Valentin Jamart [a,*], Damien Pas [a], Thierry Adatte [a], Jorge E. Spangenberg [b], Lukáš Laibl [c], Allison C. Daley [a]

[a] Institute of Earth Sciences (ISTE), University of Lausanne, CH-1015 Lausanne, Switzerland
[b] Institute of Earth surface Dynamics (IDYST), University of Lausanne, CH-1015 Lausanne, Switzerland
[c] Czech Academy of Sciences, Institute of Geology, Rozvojová 269, 165 00, Prague 6, Czech Republic

ARTICLE INFO

Editor: Dr. Bing Shen

Keywords:
Carbon isotopes
ROECE
DICE
Global correlations
Western Gondwana

ABSTRACT

The Stage 4 – lower Guzhangian interval, which includes the Drumian and Wuliuan stages is critical for understanding biogeochemical and evolutionary events of the Cambrian. It coincides with the first widespread extinction event of the Phanerozoic associated with the negative Redlichiid – Olenellid Extinction Carbon Isotope Excursion (ROECE). It marks a shift from a lower Cambrian endemic-dominated fauna to a Paleozoic-type cosmopolitan-dominated fauna, and finally, the interval includes the negative Drumian Carbon Isotope Excursion (DICE). The precise identification of the ROECE to DICE interval beyond the tropical belts has been hindered by global regression events and the limited number of geochemical studies. However, rifting in the Mediterranean subprovince of western Gondwana during this transition provides a key sedimentary record of this interval in the southern hemisphere. The Ferrals-les-Montagnes section (Montagne Noire, southern France) offers crucial stratigraphic data for defining ROECE and DICE in western Gondwana. Although significant advances have been made in biostratigraphy, the geochemical characterization of ROECE – DICE carbon isotope excursions remain insufficiently explored, posing challenges for the precise delineation of the Series 2 – Miaolingian and Wuliuan – Drumian boundaries in Montagne Noire, where diagenetic alteration has further compromised fossil preservation. This study presents new paleontological (trilobites, echinoderms), carbon stable isotope ($\delta^{13}C_{carb}$, $\delta^{13}C_{org}$), and total organic carbon (TOC) datasets from the lower to middle Cambrian Ferrals-les-Montagnes succession. These data provide the first reliable ROECE and DICE records in western Gondwana, refining the Series 2 – Miaolingian and Wuliuan – Drumian boundaries in the region, and allow refining regional and global correlations of the Miaolingian Series.

1. Introduction

The Cambrian Period is characterized by a number of key evolutionary events, including the "Cambrian Explosion" (Fig. 1A; e.g., Runnegar, 1982; Brasier, 1996; Briggs, 2015; Potin and Daley, 2023), the "Cambrian Substrate Revolution" (Fig. 1A; e.g., Seilacher, 1999; Bottjer et al., 2000; Mangano and Buatois, 2017; Buatois et al., 2018) and the onset of the "Ordovician Plankton Revolution" (Fig. 1A; Servais et al., 2008, 2016; Potin et al., 2023; Saleh et al., 2023). These evolutionary events unfolded over millions of years. The Cambrian Period is also characterized by significant carbon isotope excursions (CIEs), or anoxic events, often associated with extinctions or radiations. Notwithstanding these major changes, the Cambrian time scale remains poorly defined (Zhu et al., 2006; Babcock et al., 2007, 2015; Zhao et al., 2019) due to: (1) the scarcity of high-precision radioisotope ages (Zhu et al., 2006; Peng et al., 2020); (2) the general endemism characterizing the lower Cambrian, which makes global correlations difficult (e.g., Sdzuy et al., 1999; Gozalo et al., 2007; Fan et al., 2011; Peng et al., 2020); and (3) the paucity of well-preserved outcrops.

Ten major Cambrian Period CIEs have been identified. Their global distribution has improved intercontinental correlation (e.g., Zhu et al., 2006; Babcock et al., 2015; Álvaro, 2020; Peng et al., 2020). These CIEs

* Corresponding author.
E-mail address: Valentin.Jamart@unil.ch (V. Jamart).

https://doi.org/10.1016/j.palaeo.2025.112951
Received 11 December 2024; Received in revised form 4 April 2025; Accepted 7 April 2025
Available online 13 April 2025

are often associated with faunal radiation/extinction (Fig. 1A; e.g., Zhu et al., 2006; Peng et al., 2020), volcanism (e.g., Hough et al., 2006; Jourdan et al., 2014), and sea-level fluctuations (e.g., Babcock et al., 2015). Consequently, Cambrian CIEs are frequently employed to mark Cambrian stage boundaries (Fig. 1A; e.g., BACE, ZHUCE, ROECE, DICE, etc.; Zhu et al., 2006; Peng et al., 2020).

The correlation of two stage boundaries is of particular interest in this study. The Stage 4 – Wuliuan boundary is marked by the First Appearance Datum (FAD) of the trilobite *Oryctocephalus indicus*, which coincides with the Redlichiid–Olenellid extinction and the ROECE (Zhu et al., 2006; Peng et al., 2020). This boundary is characterized by a sea-level lowstand and unconformities, as well as by a shift from an endemic-dominated lower Cambrian communities to more Paleozoic-type cosmopolitan communities (Fig. 1A; e.g., Álvaro and Vennin, 1998; Sundberg et al., 2016; Landing et al., 2023). The Wuliuan – Drumian boundary is defined by the FAD of the cosmopolitan agnostid *Ptychagnostus atavus*. This boundary corresponds with the DICE and a global sea-level rise (i.e., Babcock et al., 2007, 2015; Li et al., 2020; Zhang et al., 2021).

The regressive sea-level phase at the Stage 4 – Wuliuan boundary, known as the Hawke Bay Regression or Event (see Álvaro and Vennin, 1998 for synonymy), had a major impact on the *circum*-Iapetus stratigraphic record (Palmer and James, 1980; Álvaro and Clausen, 2005; Landing et al., 2023). This regression, driven by an epeirogenic uplift, caused significant unconformities and hiatuses in upper Stage 4 – lower Wuliuan deposits (Palmer and James, 1980; Nielsen and Schovsbo, 2015; Landing et al., 2023), preventing identification of the ROECE for localities situated south of the paleo-equator. In contrast, the western Mediterranean region (western Gondwana) underwent a phase of tectonic rifting around the Stage 4 – Wuliuan boundary, resulting in the formation of deeper marine environments with nearly complete stratigraphic successions (Álvaro et al., 2003; Álvaro and Clausen, 2005).

In the Mediterranean area, the Ferrals-les-Montagnes section (Figs. 1B-C) represents an important sedimentary record that constrains

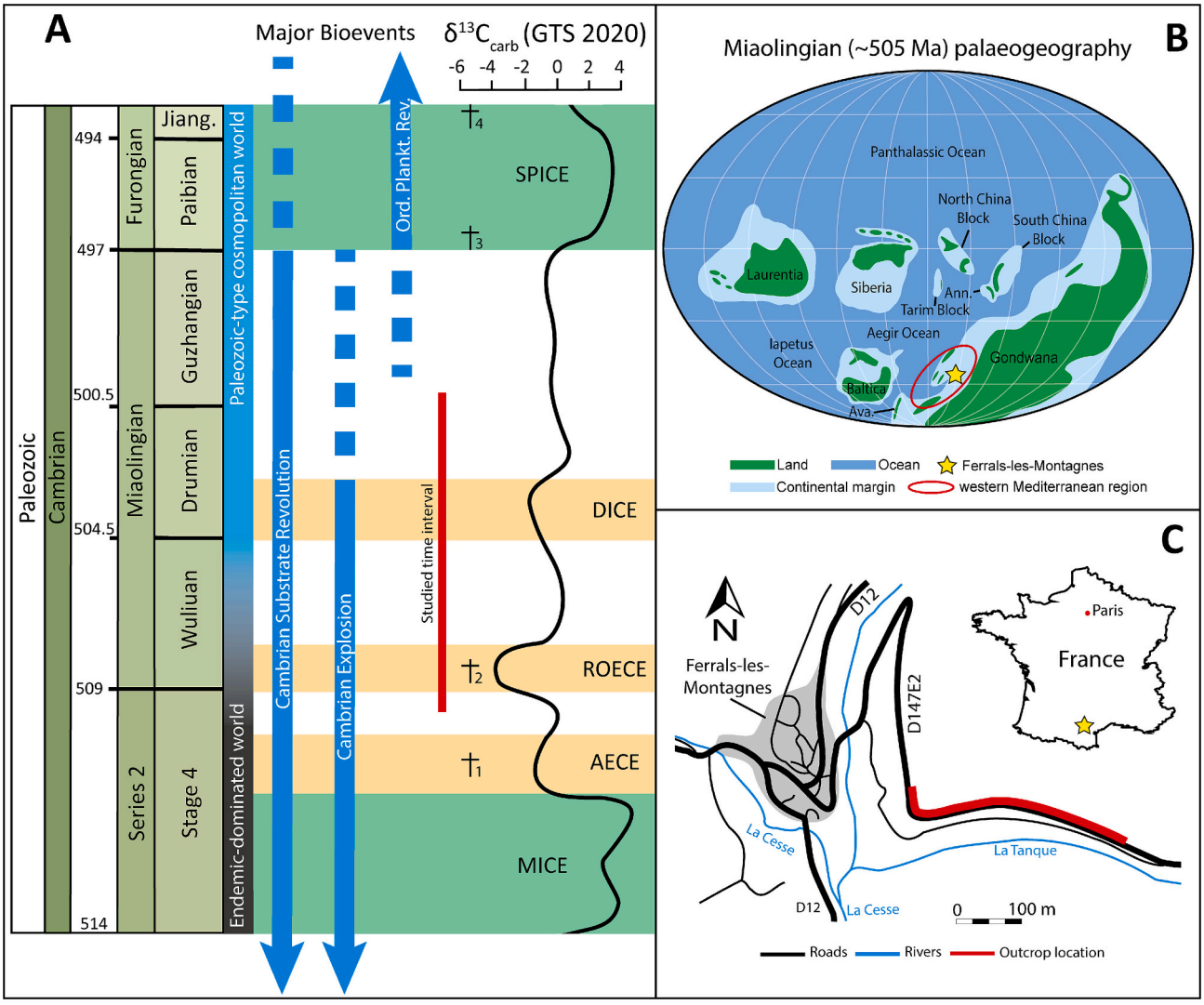

Fig. 1. Geological setting. A – Major geochemical events documented through the Series 2 to Furongian interval and the interval studied (red vertical line). B – Position of the Ferrals-les-Montagnes section along the western margin of Gondwana. C – Geographic location of the Ferrals-les-Montagnes section in southern France. The presented paleogeographic reconstruction is based on the Torsvik and Cocks (2016) GPlates model for the overall position of the continents and then modified and adapted (Mckerrow et al., 1992; Torsvik and Cocks, 2013, 2016; Scotese, 2014, 2016, 2021) for a more parsimonious localization of the continents. The stage boundaries are taken from the ICS 2023/09 chronostratigraphic chart of Cohen et al. (2013; updated). Positive CIEs are indicated in green, and negative CIEs in orange. The dagger symbols placed along the isotopic curve represent major extinction events: (1) Extinction of Archaeocyaths, (2) Extinction of Redlichiid & Olenellid trilobites, (3) Extinction of the Marjumid Biomere and Damesellid trilobites and (4) Extinction of the Pterocephalid Biomere (Peng et al., 2020). Abbreviations: Ann. = Annamia, Ava. = Avalonia, Jiang. = Jiangshanian, Ord. Plankt. Rev. = Ordovician Plankton Revolution. GPS coordinates of the section: 43.402371, 2.633431. (For interpretation of the references to colour in this figure legend, the reader is referred to the web version of this article.)

the definition of the ROECE and DICE in western Gondwana. The section is situated on the southern flank of Montagne Noire (France, Fig. 1C). The first discovery of middle Cambrian faunas in the vicinity of Ferrals-les-Montagnes is attributed to Bergeron's discovery of "primordial faunas" in 1888. Subsequently, the region became the focus of several studies, with a particular emphasis on trilobites (e.g. Álvaro and Vizcaïno, 1997, 1998; Shergold et al., 2000; Álvaro et al., 2001b) and echinoderms (Vizcaïno and Lefebvre, 1999) but also on stratigraphy (Courtessole, 1973; Álvaro et al., 1998, 2001b) and geochemistry (Wotte et al., 2007). These studies established a biostratigraphic framework for the Mediterranean subprovince, which is crucial for intercontinental correlations (Fig. 2; e.g. Gozalo et al., 2007, 2011, 2013; Geyer, 2019).

Although a few studies have focused on the carbon isotope in the Montagne Noire region (Wotte et al., 2007; Álvaro et al., 2008; Wotte et al., 2012), they have not yet definitively identified the ROECE and the DICE or precisely determined the Stage 4 – Wuliuan and Wuliuan – Drumian boundaries. The earlier event is particularly difficult to identify owing to the poor preservation of faunal assemblages caused by diagenetic overprinting.

This study describes new fossil assemblages and carbon isotope data from the 76.5 m-thick Ferrals-les-Montagnes section, and proposes an identification of the ROECE and the DICE at this location and precisely delineates the Stage 4 – Wuliuan (Series 2 – Miaolingian) and Wuliuan – Drumian boundaries. These results are correlated with the global carbon isotope framework.

2. Geological setting

During the Cambrian Period, the Montagne Noire was situated on the western margin of Gondwana at high southern latitudes and was part of the western Mediterranean region (Fig. 1B; e.g., Cocks, 2000; Álvaro and Clausen, 2005; Scotese, 2021). During late Epoch 2 the western Mediterranean basin was characterized by a succession of mixed carbonate-siliciclastic platform deposits that rapidly disappeared around the Age 4 – Wuliuan boundary, owing to the onset of a rifting tectonic phase (Álvaro and Vennin, 1996; Demange, 2001; Álvaro et al., 2013).

The Montagne Noire is commonly divided into three distinct zones. 1) The northern flank is composed of a slightly metamorphized succession of sedimentary rocks, ranging from the lower Cambrian to the Silurian (Gèze, 1949; Demange, 2001; Devaere et al., 2013). 2) The Axial zone consists of metamorphic rocks (e.g., domes of gneiss, migmatites and micaschists, Gèze, 1949; Demange, 2001; Devaere et al., 2013). 3) The southern flank comprises a complete lower Cambrian – lower Carboniferous succession of nearly 3000 m-thick carbonate and siliciclastic deposits (Gèze, 1949; Álvaro and Vizcaïno, 2001; Demange, 2001; Devaere et al., 2013). The Ferrals-les-Montagnes section is a 76.5 m thick interval located in the southern flank, extending from Stage 4 (*Acadoparadoxides mureroensis* Biozone) to the lower Guzhangian (*Lejopyge laevigata* Biozone), and encompassing the Pont de Poussarou, La Tanque, Coulouma, and Ferrals formations (Fig. 2).

The Pont de Poussarou Formation (PDP; Figs. 2, 3, 4C-G) is ~32 m-thick and shows two main facies. The lower part of the formation is characterized by massive, white limestone with intermittent dolostone layers, representing deposition within an outer carbonate platform setting (Álvaro and Vennin, 1996; Álvaro et al., 1998; Demange, 2001). The upper part of the formation, which transitions toward the La Tanque Formation, exhibits a gradual increase in reddish argillaceous compounds (Álvaro et al., 1998). This transition is concluded by the occurrence of white limestone/dolostone nodules floating in a purple shaly matrix, similar to the Griotte lithology (Álvaro et al., 1998).

The deposition of this transitional facies correlates with a deepening of the platform during the late Age 4 to early Drumian interval (Álvaro and Vennin, 1996; Demange, 2001). The drowning of the platform is associated with a diachronous rifting phase (Álvaro and Vennin, 1996; Álvaro et al., 2010b, 2013), which resulted in significant lateral variations in the PDP formation, as well as the La Tanque (LTQ) and Coulouma (COU) formations, which are discussed in more detail below. The PDP formation is believed to correlate with the uppermost Stage 4/lower

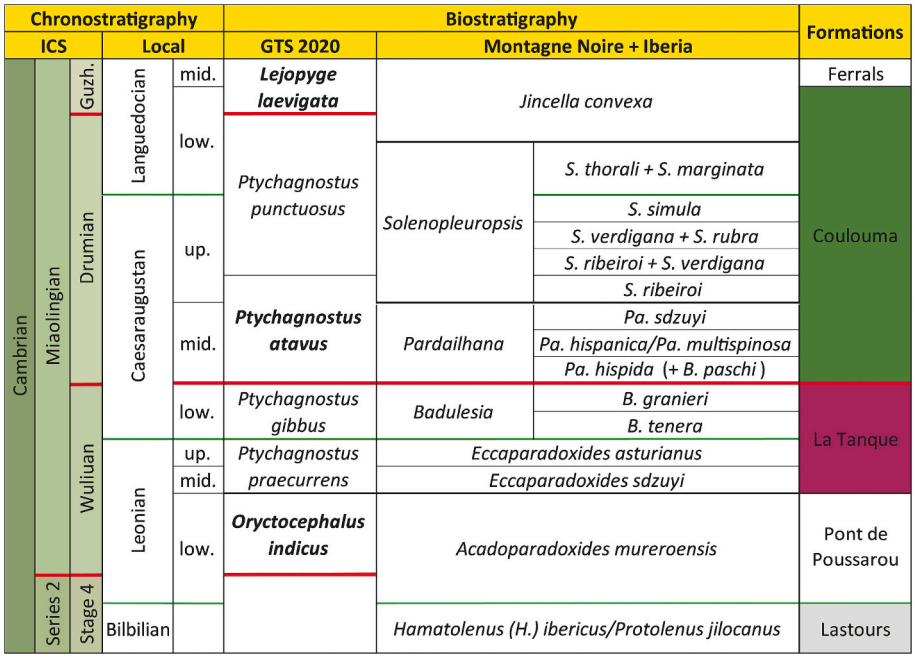

Fig. 2. Biostratigraphic framework established for Montagne Noire and Iberia in comparision to the global (GTS) biostratigraphic framework and its correlation with the formations present in the Ferrals-les-Montagnes section. Fossil species in bold correspond to index taxa used to delineate Cambrian stage boundaries. The bold red lines mark stages boundaries. The green lines represent local stage boundaries of the Mediterranean subprovince. Abbreviations: B. = *Badulesia*, Guzh. = Guzhangian, H. = *Hamatolenus*, low. = lower, mid. = middle, Pa. = *Pardailhana*, S. = *Solenopleuropsis*, up. = upper. Figure based on data from Álvaro et al. (1998, 2020), Álvaro and Vizcaïno (2000), Álvaro and Clausen (2005), Gozalo et al. (2007, 2011, 2013), Wotte et al. (2007), and Geyer (2019). (For interpretation of the references to colour in this figure legend, the reader is referred to the web version of this article.)

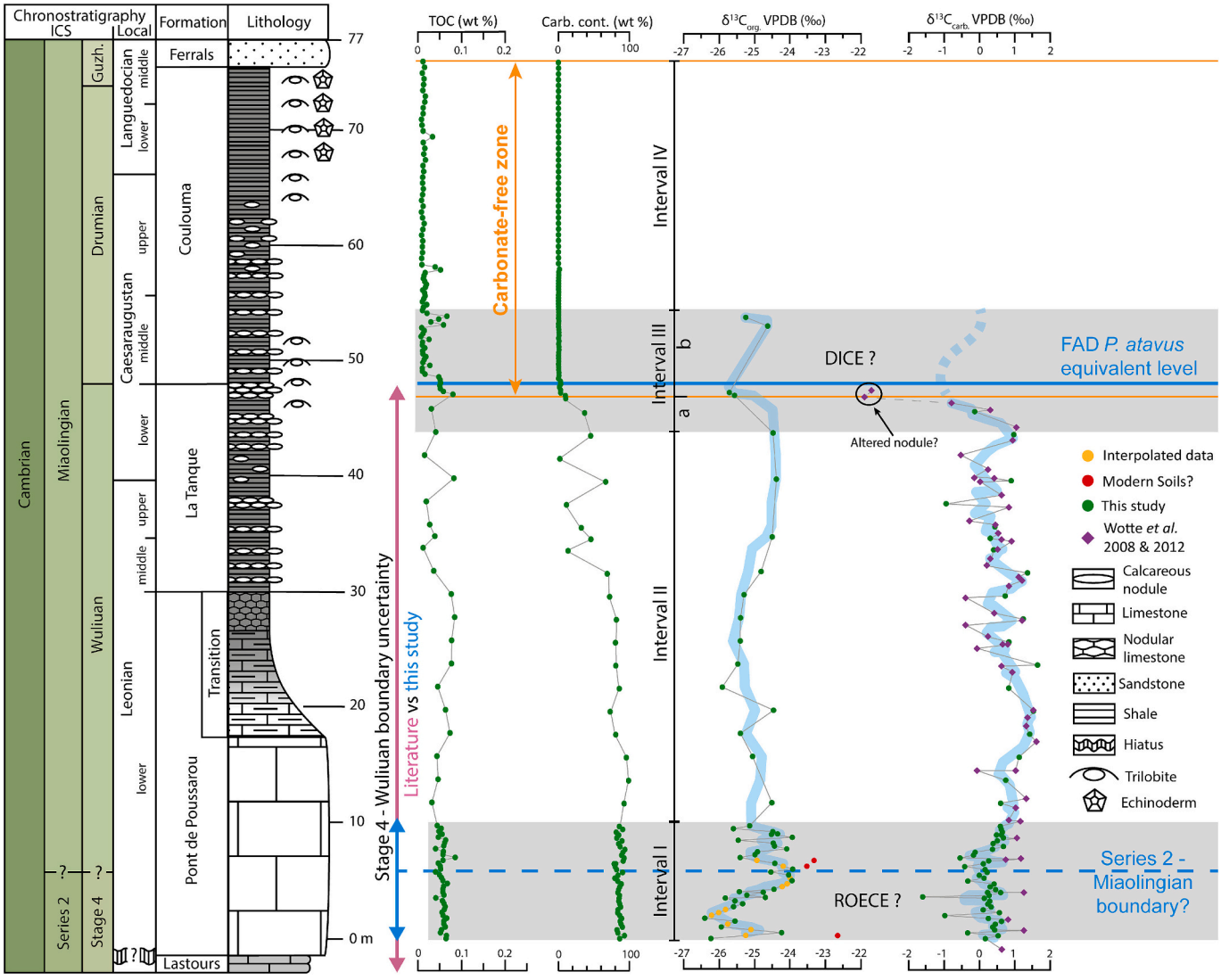

Fig. 3. Stratigraphic column, TOC, Carbonate content (Carb. cont.) and carbon isotopes of the Ferrals-les-Montagnes section. The gray colour in the lithological columns reflects the relative proportion of argillacaeous content in the rocks. The vertical purple (literature) and blue (this study) double-headed arrows correspond to the uncertainty in the position of the Series 2 – Miaolingian boundary. The vertical blue curves represent the 3-points moving average trend of $\delta^{13}C_{org}$ and $\delta^{13}C_{carb}$. The horizontal blue dashed line represents the proposed location of the Series 2 – Miaolingian boundary, which is consistent with the positioning proposed by Wotte et al. (2012). The horizontal solid blue line represents the *B. granieri/P. hispida* boundary, which is conterminous with the FAD of *P. atavus* (i.e. Gozalo et al., 2011; Geyer, 2019). The horizontal gray shadings correspond to the ROECE and DICE intervals. The horizontal solid orange lines delineate the carbonate-free zone in the upper part of the stratigraphic column. The global chronostratigraphic chart is derived from Cohen et al. (2013; updated). The local chronostratigraphy is adapted from Álvaro et al. (1998). Abbreviations: Guzh. – Guzhangian. (For interpretation of the references to colour in this figure legend, the reader is referred to the web version of this article.)

Wuliuan (lower Leonian)(Fig. 2; Álvaro et al., 2014, 2020; Geyer, 2019). From a biostratigraphic perspective, this interval correlates with the *Acadoparadoxides mureroensis* Biozone (Álvaro and Clausen, 2005; Gozalo et al., 2007, 2013). However, the lack of precise biostratigraphic control and the effects of diagenesis in the Ferrals-les-Montagnes section hinder an accurate identification of the first occurrence (FO) of *A. mureroensis*, thereby limiting the precision of biostratigraphic constraints on the PDP Formation (Álvaro and Vizcaïno, 1998; Álvaro et al., 2000; Álvaro and Clausen, 2005).

The La Tanque Formation (LTQ; Figs. 2, 3, 4G-J) is 18.75 m-thick and is characterized by Griotte-like facies. In the Ferrals-les-Montagnes section, the formation is composed of centimeter-thick alternations of bioclastic limestone/dolostones and reddish to purple shales (see Álvaro et al., 1998 for more details). This facies is widely distributed throughout the lower-middle Cambrian transition interval of the western margin of Gondwana (Álvaro and Vennin, 1996; Álvaro et al., 2001b; Álvaro and Clausen, 2005). The formation spans an interval extending from the lower Wuliuan (middle Leonian) to the lower Drumian Stage boundary (middle Caesaraugustan) (Fig. 2; Álvaro et al., 1998, 2001b; Gozalo et al., 2011; Geyer, 2019). This time interval corresponds to the middle *Oryctocephalus indicus* (*Eccaparadoxides sdzuyi*) – *Ptychagnostus atavus* (*Pardailhana hispida*) biozones (Álvaro and Vizcaïno, 1998; Álvaro et al., 2001b; Gozalo et al., 2011; Geyer, 2019).

The Coulouma Formation (COU; Figs. 2, 3, 4J) is 27 m-thick and consists of green (locally lie-de-vin) shales containing carbonaceous (limestone to dolostone) nodules (see Álvaro et al., 1998 for more details). This formation spans an interval extending from the Drumian (lower Caesaraugustan) to the lower Guzhangian (middle Languedocian) (Fig. 2; Álvaro et al., 1998, 2001b; Geyer, 2019). This interval corresponds to the *Pt. atavus* (*Pa. hispida*) – *Lejopyge laevigata* (*Jincella convexa/J.*? cf. *prantli*) biozones (Álvaro and Vizcaïno, 1998; Álvaro et al., 1999, 2004; Geyer, 2019).

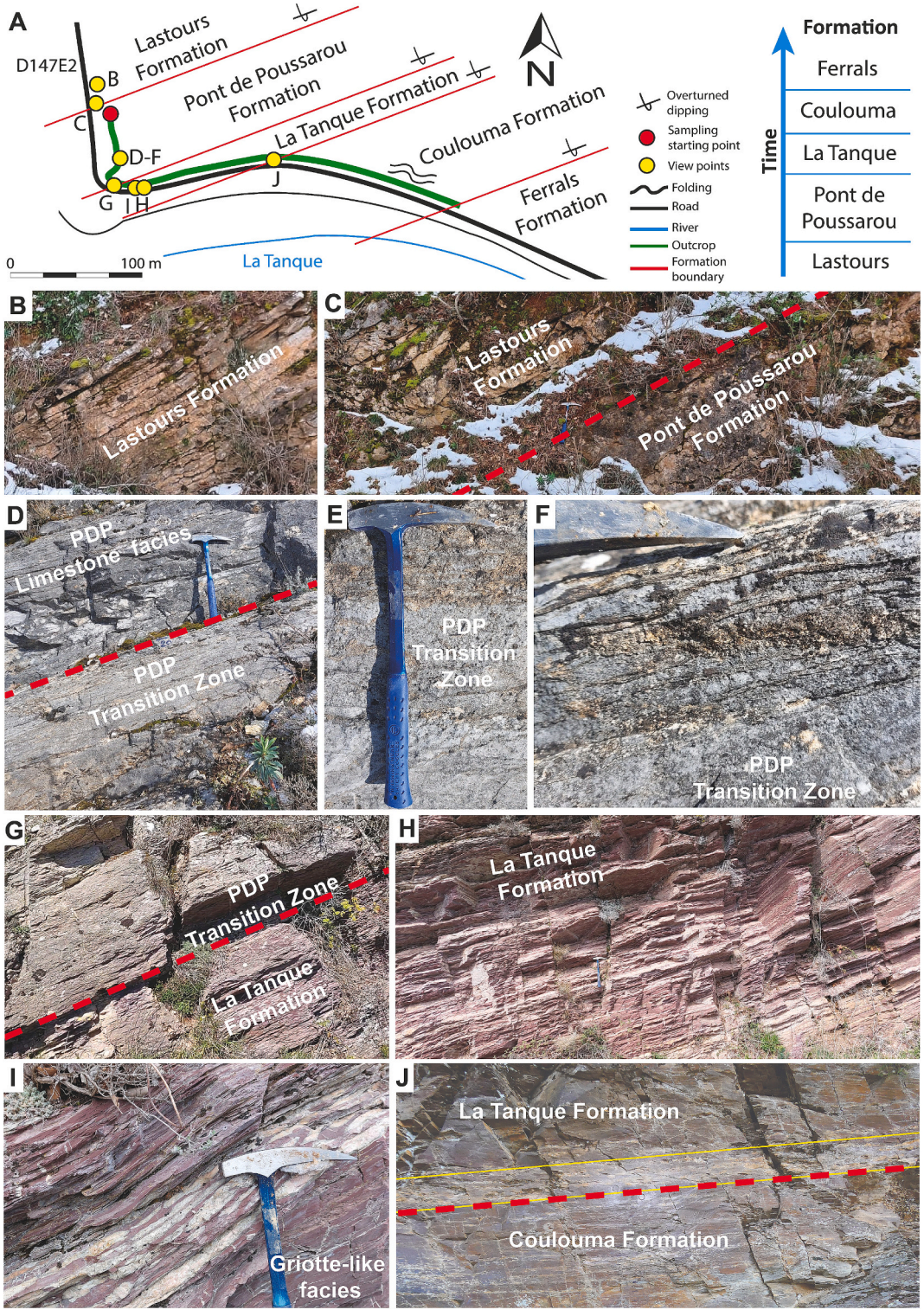

Fig. 4. Field observations along the Ferrals-les-Montagnes section. A – Location of field views through the studied interval. B – Platy limestone of the upper Lastours Formation. C – Boundary between Lastours and Pont de Poussarou formations. D – Start of the transition zone between Pont de Poussarou and La Tanque formations. *E*-F – Close-up of the transition zone and the increase in argillaceous content. G – Boundary between Pont de Poussarou and lower part of the La Tanque formations, corresponding to the top of the transition zone. H – Griotte-like facies characteristic of the La Tanque Formation. I – Close-up of the Griotte-like facies. J – Green shales marking the boundary between La Tanque and Coulouma formations. The boundary (red dashed line) is marked by a 20 cm-thick accumulation of altered orangish limestone/dolomite nodules (delineated by yellow lines). Length of hammer is 38 cm. (For interpretation of the references to colour in this figure legend, the reader is referred to the web version of this article.)

The Ferrals Formation (FRL; Figs. 2, 3) is up to 500 m-thick and consists of gray to white sandstones (see Álvaro et al., 1998 for more details). The lower part of the formation is of Guzhangian age (middle Languedocian) (Fig. 2; Álvaro and Vizcaïno, 1998; Geyer, 2019), which corresponds to the *L. laevigata* (*J. convexa/J.*? cf. *prantli*) Biozone (Geyer, 2019). The sampling in this study is limited to the first meter of this formation.

3. Materials and Methods

3.1. Sampling

The Ferrals-les-Montagnes section was sampled (Fig. 3) at 2 m resolution in the carbonate-dominated interval of the section (0–48.75 m) and at 50 cm in the siliciclastic-dominated interval (48.75–76.5 m). Expected ROECE and DICE intervals were sampled at 25 cm resolution over 10 m. Our sampling resolution ensures a reliable correlation with the works of Wotte et al. (2007, 2012), and significantly increases the sample resolution for the expected ROECE and the DICE. In total, 144 samples were collected for TOC and $\delta^{13}C$ analyses (Supplementary Materials 1). GPS coordinates for the starting point of sampling: 43.402371, 2.633431.

To improve the quality of the biostratigraphic correlations of this section, 58 fossil specimens were collected in the LTQ and COU formations (samples belongs to the Musée Cantonal de Géologie (MGL), Lausanne and are stored at the University of Lausanne).

3.2. Microfacies observations

Seven thin sections were prepared to illustrate the microfacies of each formation in the section. A brief description of each thin section can be found in Supplementary Materials 2.

3.3. Geochemical proxies

All collected samples were powdered from carefully selected and cleaned rocks free of calcite veins and analyzed for TOC and $\delta^{13}C$.

3.4. Rock-Eval pyrolysis (TOC, Carbonate contents, HI, OI)

Organic matter (OM) analyses were performed on whole-rock powdered samples using a Rock-Eval 6 at the Institute of Earth Sciences, University of Lausanne, following the method described by Espitalié et al. (1985) and Behar et al. (2001). Measurements were calibrated using the IFP 160000 standard. Rock-Eval pyrolysis provides parameters, such as hydrogen index (HI, mg HC/g TOC, HC = hydrocarbons), oxygen index (OI, mg CO_2/g TOC), T_{max} (°C), and the TOC content (wt%). HI, OI and T_{max} values, which give an overall measure of the type and maturation of the organic matter (e.g., Espitalié et al., 1985), were interpreted for TOC $\geq$ 0.2 wt% and S_2 values $\geq$0.2 mg HC/g.

3.5. Carbon and oxygen stable isotopes ($\delta^{13}C_{carb}$, $\delta^{13}C_{org}$, $\delta^{18}O$)

Out of the 144 samples, 61 samples were selected (i.e. carbonate content >10 wt%) for carbonate carbon and oxygen stable isotopes ($\delta^{13}C_{carb}$ and $\delta^{18}O$ values). Aliquots of the rock powders were reacted with 100 % phosphoric acid at 70 °C using a Gasbench II connected to a Thermo Fisher Delta V Plus mass spectrometer. All values are reported in per mil relative to Vienna Pee Dee belemnite limestone standard (VPDB). Reproducibility and accuracy were monitored by replicate analyses of laboratory standards that had been calibrated against international standards, specifically NBS19 ($\delta^{13}C$ = +1.95 ‰, $\delta^{18}O$ = −2.2 ‰), NBS18 ($\delta^{13}C$ = −5.01 ‰, $\delta^{18}O$ = −23.01 ‰), and IAEA-CO9 ($\delta^{13}C$ = −47.32 ‰, $\delta^{18}O$ = −15.28 ‰); $\delta^{13}C$ and $\delta^{18}O$ values from Brand et al. (2014). Reproducibility for $\delta^{13}C$ and $\delta^{18}O$ were better than ±0.04 ‰ and ± 0.10 ‰ (1 std. dev.), respectively. Replicate analyses of NBS 19 were used for quality control of the measurements.

The organic carbon stable isotope compositions ($\delta^{13}C_{org}$ values, ‰ vs. VPDB) were determined in 52 decarbonated samples with TOC content <0.1 wt% (up to 0.03 wt% for samples with carbonate content >20 wt%) by elemental analysis and isotope-ratio mass spectrometry (Spangenberg and Herlec, 2006). The used EA/IRMS system at the Institute of Earth Surface Dynamics of the University of Lausanne (UNIL, IDYST) consisted of a Carlo Erba 1108 (Fisons Instruments, Milan, Italy) elemental analyzer connected to a Delta V Plus isotope-ratio mass spectrometer via Con-Flo III split interface (both of Thermo Fisher Scientific, Bremen, Germany) operated under continuous helium flow. Before analysis the samples were decarbonated by treatment with 10 % *v*/v HCl, thoroughly washed with deionized water, and dried (40 °C, 48 h). The calibration and normalization of the measured $\delta^{13}C$ values to the VPDB scale were performed using a 3-point calibration with international reference materials and UNIL in-house standards (details on the standards in Spangenberg, 2024). The repeatability and intermediate precision were better than 0.1 ‰ for $\delta^{13}C_{org}$. In the case of the carbonate-rich sample (> 10 % carbonate content), the recalculation of the TOC following the acid attack (carbonate removal) demonstrated that a higher quantity of organic carbon was present in the sample than was observed during the Rock-Eval 6 pyrolysis. This enabled the analysis of carbonate-rich samples with low Rock-Eval 6 TOC values (up to 0.03 wt%).

In addition, we examined the influence of calcite veins on the whole rock $\delta^{13}C_{carb}$ analysis (Supplementary Materials 2). To do so, we compared whole rock $\delta^{13}C_{carb}$ values of selected samples with values obtained for specific spots (calcite and micrite) within the same samples. These spots were selected and drilled based on thin section counterparts after petrographic observations. Aliquots of the rock powders were measured following the same protocol as described above for the whole rock measurements.

3.6. Elemental geochemistry

To complement our evaluation of diagenetic impact on the preservation of the isotopic signal, we measured a total of 30 samples for elemental geochemistry. Measurements were conducted using a Brucker Tracer 5 g portable X-ray fluorescence (pXRF) device hosted at the University of Liège (ULiège). Samples were measured with the Oxide3-phase method with an elapsed time of 60 s (see Da Silva et al., 2023 for further details concerning the pXRF settings). To calculate the elemental Mg phase, the MgO phase obtained through the pXRF measurements was converted into elemental phase using the oxide-to-element conversion factor of 1.658 (conversion factor is from the Advanced Analytical Center, James Cook University, Australia).

All the data obtained are presented in wt% (Supplementary Materials 1) but to facilitate comparison with the data from Wotte et al. (2012), they were converted to ppm. The pXRF data are available in Supplementary Materials 1 (data) and Supplementary Materials 2 (data description and interpretation).

4. Results

4.1. Biostratigraphy

The trilobites from the studied section are typical representatives of the traditional middle Cambrian taxa from West Gondwana, especially members of Solenopleuridae Angelin, 1854, Conocoryphidae Angelin, 1854, and Paradoxididae Hawle and Corda, 1847. The lowest trilobite occurrences are found between 46.5 and 51.25 m above the base and are represented by several conocoryphid cranidia, including *Conocoryphe herberti* Munier-Chalmas et al., 1889 (Fig. 5D) and *Ctenocephalus* cf. *bergeroni* Thoral, 1946 (Fig. 5I). Other trilobites present in this interval include paradoxidids such as *Eccaparadoxides rouvillei* (Miquel, 1905)

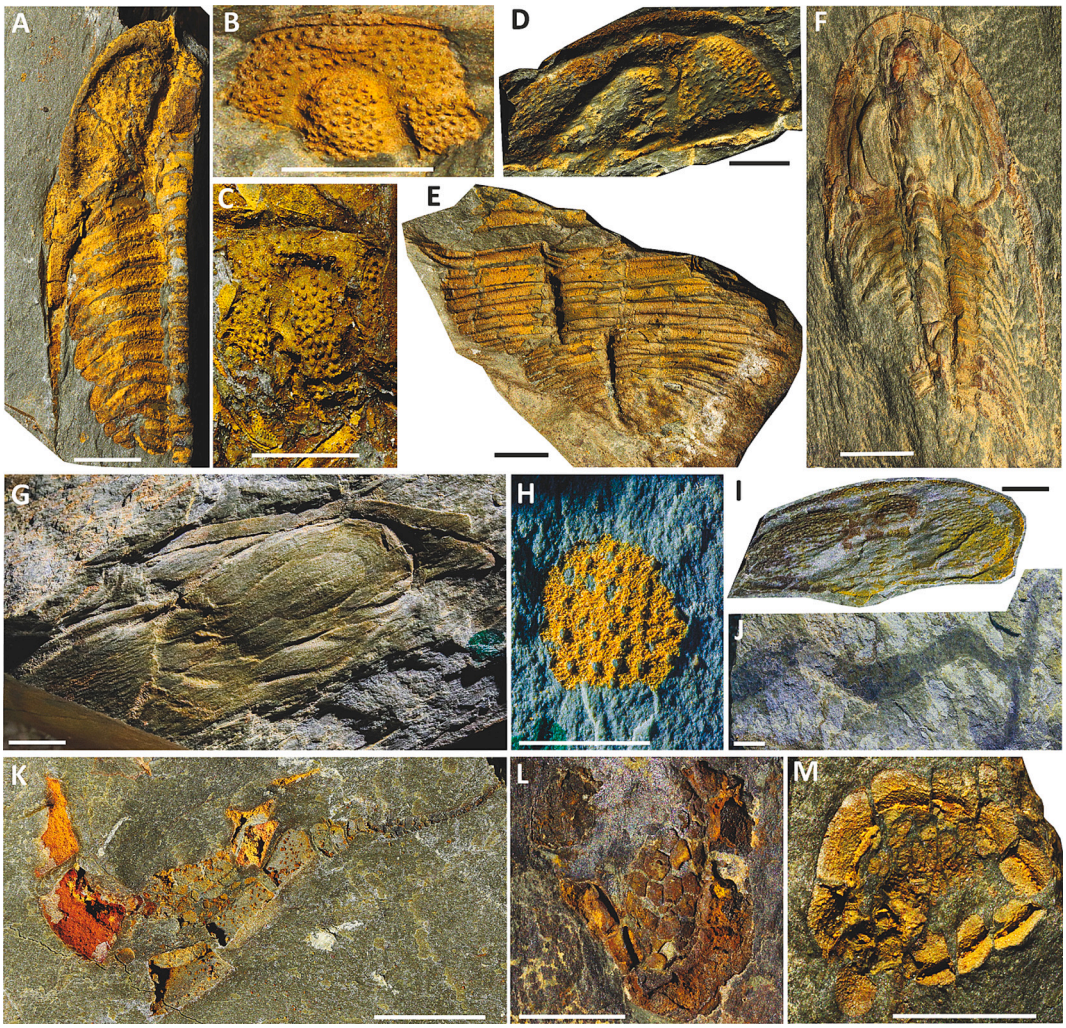

Fig. 5. Trilobites, echinoderms, and other fossils from the Ferrals-les-Montagnes section. A – *Ctenocephalus antiquus* Thoral, 1946; MGL 110498. B – *Solenopleuropsis* cf. *rouayrouxi* Munier-Chalmas et al., 1889; MGL 110499. C – *Solenopleuropsis* cf. *multigranifera* Thoral, 1948; MGL 110500. D – *Conocoryphe herberti* Munier-Chalmas et al., 1889; MGL 110501. E – Isolated fragment of conocoryphid thorax; MGL 110502. F – *Eccaparadoxides mediterraneus* (Pompeckj, 1901); MGL 110503. G – *Eccaparadoxides rouvillei* (Miquel, 1905); MGL 110504. H – Sclerite fragment of trilobite; MGL 110505. I – *Ctenocephalus* cf. *bergeroni* Thoral, 1946; MGL 110506. J – Possible algae; MGL 110507. K – Indet. Cinctan echinoderms (*Sucosytis*?); MGL 110508. L – Cinctan indet; MGL 110509. M – *Sucosytis theronensis* Cabibel et al., 1959; MGL 110510. Scale bars = 5 mm.

(Fig. 5G). The next record is an almost complete individual of *Ctenocephalus antiquus* Thoral, 1946 from 64.45 m above the base (Fig. 5A). The interval between 64 and 71.25 m above the base contains numerous cranidia belonging to the genus *Solenopleuropsis*, including *S.* cf. *rouayrouxi* Munier-Chalmas et al., 1889 and *S.* cf. *multigranifera* Thoral, 1948 (Figs. 5B-C), as well as an isolated fragment of a conocoryphid thorax (Fig. 5E). The top of the section, 71.75 m above the base and higher, contains fragmentary cranidia and one nearly complete articulated individual (Fig. 5F) of *Eccaparadoxides mediterraneus* (Pompeckj, 1901).

The echinoderms from the studied section have been identified as belonging to the typical and diversified middle Cambrian Cinctan group (Smith and Zamora, 2009) based on their morphology, which lacks radial symmetry. However, except for one specimen identified as *Sucosytis theronensis* Cabibel et al., 1959, a precise generic or specific identification of the collected samples was not possible (Figs. 5K-M).

In addition, remains that were interpreted as potential algae and sclerites of trilobites were collected in the 46.5–51.25 m interval (Fig. 5H, J).

4.2. Microfacies

Illustrations of microfacies and the location of samples used for thin section are available in Supplementary Materials 2. The microfacies from the PDP Formation are characterized by mudstone to wackestone texture, showing rare to abundant bioclasts of diverse origins in a gray micritic matrix. Infra-millimetric to millimetric sized clay veinlets, crystallised cavities and a few calcite veins are present. The thin sections from the LTQ Formation exhibit microfacies characterized by a red colour matrix, occasional white colour limestone nodules, rare to absent bioclasts, and rare infra millimetric dolomite crystals. The COU Formation shows microfacies characterized by a greenish to brownish matrix and dispersed infra millimetric white quartz grains. The FRL Formation microfacies is characterized by quartz arenite with a syntaxial overgrowth cement.

4.3. Geochemistry

4.3.1. Rock-Eval pyrolysis (TOC, Carbonate contents, HI, OI)

TOC contents of the measured samples range from 0.01 to 0.09 wt% with a mean value of 0.03 wt% (Fig. 3). The HI values of the measured

samples range from 0 to 518 mg HC/g TOC (Fig. 6C). The OI of the measured samples range from 139 to 1697 mg CO_2/g TOC (Fig. 6C).

The carbonate contents of the measured samples range from 0.1 to 100 wt% (Fig. 3). The values range from 70 to 100 wt% for the PDP Formation. For the LTQ Formation, the increase of argillaceous content induced a strong variability (sawtooth diagram) with values ranging from 0.5 to 70 wt%. For the COU Formation, all the values are <10 wt% and range from 0.2 to 2 wt% due to the dominance of the argillaceous content. For the FRL Formation, the single measured point has a carbonate content of 0.1 wt%.

4.3.2. Carbon and oxygen stable isotopes ($\delta^{13}C_{carb}$, $\delta^{13}C_{org}$, $\delta^{18}O$)

The Ferrals-les-Montagnes section is subdivided into four intervals (Fig. 3) as follows: Interval I extends from 0 to 10 m, Interval II extends from 10 to 44 m, Interval III extends from 44 to 55 m and Interval IV extends from 55 to 77 m. Interval III is subdivided into "Interval III a", corresponding to the lower carbonate-dominated part of the section, and "Interval III b", corresponding to the upper siliciclastic-dominated (carbonate-free) part of the section.

The $\delta^{13}C_{carb}$ values range from −1.66 ‰ to +1.53 ‰ in intervals I-III, with a mean value of +0.32 ‰ (Fig. 3). In interval I, a negative $\delta^{13}C_{carb}$ excursion is followed by a rapid recovery to higher $\delta^{13}C_{carb}$ values. The baseline $\delta^{13}C_{carb}$ value of the excursion is approximately +0.5 ‰, with an amplitude variation of ~1 ‰. The maximum value of about −0.5 ‰ is observed at 3.8 m (Fig. 3). In interval II, the $\delta^{13}C_{carb}$ value increases gradually from the baseline of +0.5 ‰ up to a maximum of +1.5 ‰ before gradually decreasing to the baseline value. In interval III a, the single $\delta^{13}C_{carb}$ data point is −0.2 ‰. In intervals III b and IV, the carbonate content is too low (< 10 wt%) to produce $\delta^{13}C_{carb}$ data.

The $\delta^{13}C_{org}$ values for the Ferrals-les-Montagnes section range from −26.4 ‰ to −22.7 ‰, with a mean value of −24.8 ‰ (Fig. 3). In interval I, a pronounced negative excursion in $\delta^{13}C_{org}$ is followed by a rapid recovery to higher values. The baseline $\delta^{13}C_{org}$ value of the excursion is roughly −24 ‰, with an amplitude variation of ~2 ‰ and a maximum value of −26.5 ‰ at 2 m. In interval II, the $\delta^{13}C_{org}$ values stabilized at a mean value of ~ − 25 ‰. In interval III, the few $\delta^{13}C_{org}$ values exhibit a pronounced negative $\delta^{13}C_{org}$ excursion centered at 48.5 m, with a peak value of −25.7 ‰. The baseline $\delta^{13}C_{org}$ value of the excursion is approximately −24.4 ‰, with an amplitude variation of ~1.3 ‰ (Fig. 3). $\delta^{13}C_{org}$ data could not be produced for interval IV due to the low TOC content (< 0.05 wt%).

The $\delta^{18}O$ values range from −18.5 ‰ to −9.5 ‰ for the entire section, with a mean value of −16.4 ‰ (see Supplementary Materials 1).

4.3.3. X-ray Fluorescence

This study focused on the Mn/Sr, Mg/Ca, Sr/Ca, and Mn/Ca ratios, with a detailed discussion provided in Supplementary Materials 1.

5. Discussion

5.1. Biostratigraphy

The identified trilobite taxa, *C. antiquus* (*Pardailhania hispida* Biozone to lower *Solenopleuropsis* superzone), *Solenopleuropis* species (*Solenopleuroposis* superzone), and *E. mediterraneus* (*Solenopleuropsis* superzone to *Jincella convexa* Biozone), indicate a correlation with the middle

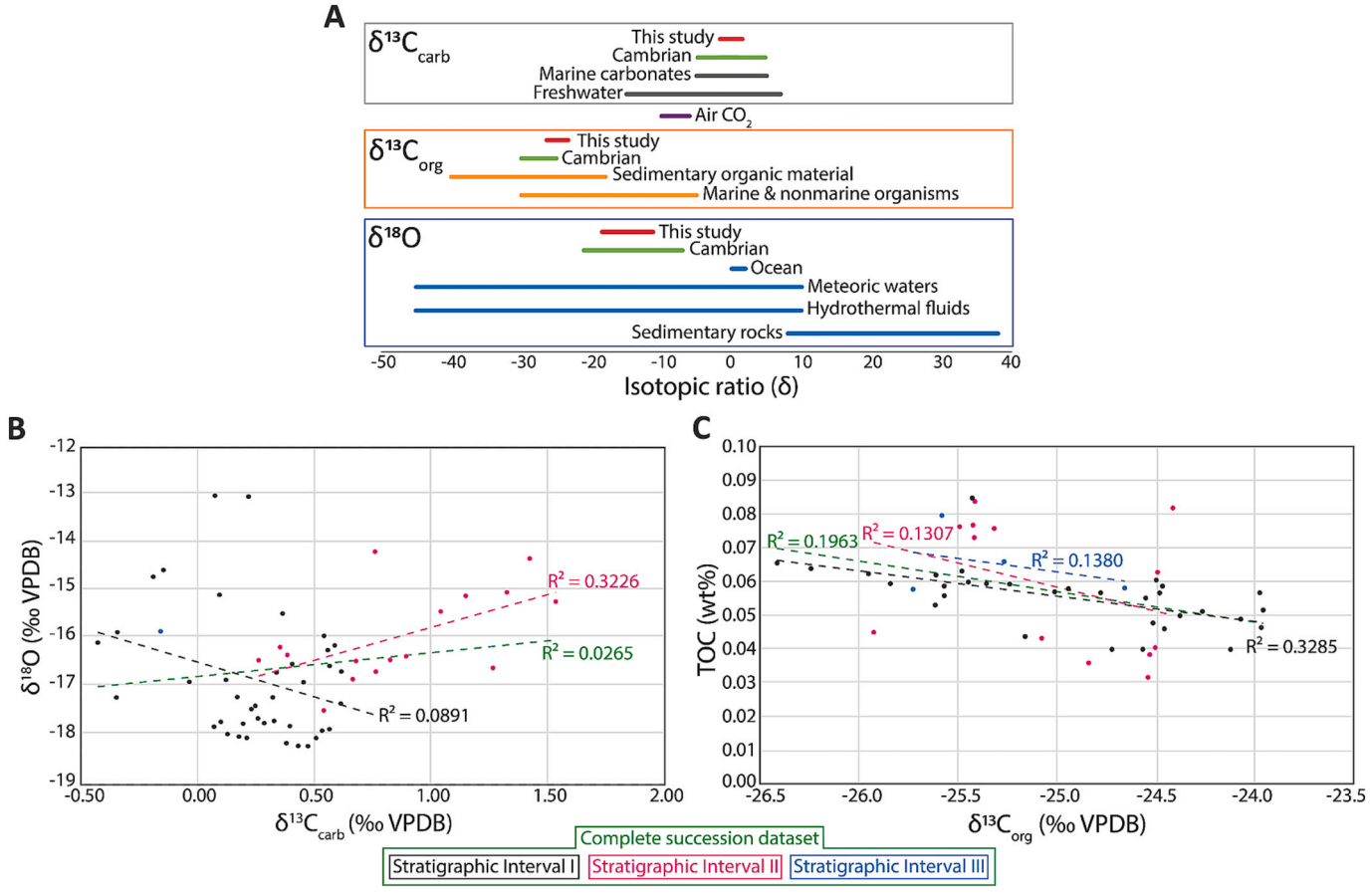

Fig. 6. Geochemistry and signal preservation. A – Comparison of the $\delta^{13}C$ and $\delta^{18}O$ isotopes between the Ferrals-les-Montagnes section (this study), the Cambrian expected range of isotopic values (Veizer et al., 1999; Krissansen-Totton et al., 2015; Sharp, 2017; Lin et al., 2019; Cramer and Jarvis, 2020) and the isotopic values for different geochemical reservoirs (Hoefs, 2021). B – Comparison between $\delta^{13}C_{carb}$ and $\delta^{18}O$. C – Comparison between $\delta^{13}C_{org}$ and TOC. The suspected modern soil data points have not been considered for the graphs in B and C.

or upper Caesaraugustian up to the middle Languedocian (cf. Courtessole, 1973; Álvaro and Vizcaïno, 1998; Gozalo et al., 2011). These levels correspond to the global Drumian Stage (Geyer, 2019).

The identified echinoderm specimen (*Sucosytis theronensis* Cabibel et al., 1959) indicates a late Drumian to early Guzhangian age. Concerning the other collected specimens (Levels E and F of Courtessole, 1973), they should, according to Vizcaïno and Lefebvre (1999), belong to the species *Elliptocinctus barrandei* (Munier-Chalmas et al., 1889) (early Drumian – early Guzhangian), *Sucocystis bretoni* Friedrich, 1993 (early Guzhangian), *S. theronensis* Cabibel et al., 1959 (late Drumian – early Guzhangian) or *Gyrocystis platessa* Jaekel, 1918 (early Drumian – early Guzhangian). The interval during which these four species are present extends from the late Drumian to the early Guzhangian (Smith and Zamora, 2009).

5.2. Geochemistry and signal preservation

The Montagne Noire area has been subject to diagenesis and low-grade metamorphism up to 300 °C (Montmartin et al., 2021). These processes can overprint the primary geochemical signal (e.g. Irwin et al., 1977; Kaufman and Knoll, 1995) and therefore it is important to assess the impact of diagenesis and metamorphism in the investigated section. To do so, we have combined data from rock-eval pyrolysis and isotope geochemistry, along with data from thin sections, which are described and interpreted in Supplementary Materials 2.

The preservation of the $\delta^{13}C_{carb}$ signal was evaluated through its correlation with $\delta^{18}O$ (Kaufman and Knoll, 1995; Chang et al., 2017; Álvaro, 2020). The lack of correlation between $\delta^{13}C_{carb}$ and $\delta^{18}O$ ($R^2 < 0.32$, Fig. 6C) suggests a weak diagenetic-metamorphic overprint. This lack of correlation should be regarded carefully as the $\delta^{18}O$ values are very negative (ranging from −18.5 ‰ to −11.2 ‰, Fig. 6A). However, in agreement with the observations of Wotte et al. (2012), the $\delta^{13}C_{carb}$ signature appears to have been only weakly overprinted. Furthermore, $\delta^{13}C_{carb}$ is generally considered to be relatively robust to diagenesis and low-grade metamorphism (e.g., Kaufman and Knoll, 1995; Álvaro et al., 2008; Wotte et al., 2012).

In order to assess the preservation of the primary $\delta^{13}C_{org}$ signal, it is recommended to examine the correlation between the $\delta^{13}C_{org}$ and TOC values (Kaufman and Knoll, 1995; Álvaro, 2020; Li et al., 2020). The low correlation coefficient between the $\delta^{13}C_{org}$ and TOC ($R^2 = 0.20$, Fig. 6D) suggests that the $\delta^{13}C_{org}$ signal is preserved. This conclusion is also valid when examining the specific intervals I, II and III, for which the correlation coefficient values are below 0.33.

The HI/OI ratio and T_{max} can be used to estimate the thermal maturity of the organic carbon data (Peters, 1986). The generally low TOC content (< 0.1 wt%) in the section is attributed to the low-grade metamorphism that has affected the Montagne Noire region. This process resulted in the loss of almost all the organic matter due to thermal maturation, although the original TOC content may have been >1 wt% (Raiswell and Berner, 1987; Álvaro, 2020). As a result, the rock-eval parameters other than TOC and carbonate contents are unusable.

The $\delta^{13}C_{carb}$ values for the section fall within the range of values recorded for the Cambrian Period (Fig. 6A; Veizer et al., 1999; Sharp, 2017; Cramer and Jarvis, 2020) and align with the −5 ‰ to +5 ‰ range reported for carbonate reservoirs (Hoefs, 2021). The $\delta^{13}C_{carb}$ trend observed in the Ferrals-les-Montagnes are also consistent with those reported in the GTS 2020 for the time equivalent interval (Peng et al., 2020).

The $\delta^{13}C_{org}$ values recorded in Ferrals-les-Montagnes fall within the expected range of Cambrian values indicating a limited metamorphic imprint on the organic carbon isotopes (Krissansen-Totton et al., 2015; Sharp, 2017; Fig. 6A). We believe that the $\delta^{13}C_{org}$ values heavier than −24 ‰ are contaminated by modern organic carbon (−30 ‰/−5 ‰; Hoefs, 2021) and they will not be discussed further.

As anticipated, the low-grade metamorphism of the studied succession and associated thermal maturation/fluid interactions have significantly impacted the oxygen isotopic signal. The $\delta^{18}O$ values in our dataset (ranging from −18.5 ‰ to −11.2 ‰, Fig. 6A) fall within the range of values for meteoric water and hydrothermal fluids reservoirs (e.g., Hoefs, 2021), indicating an overprint by post-depositional processes (see details in Kaufman and Knoll, 1995; Chang et al., 2017; Álvaro, 2020).

According to Álvaro et al. (2008), these post-depositional processes in Montagne Noire may have slightly depleted the absolute values of the $\delta^{13}C$ signal but they did not significantly alter the carbon isotopic signal. Thus, the trends observed in the $\delta^{13}C$ signal remain reliable for chemostratigraphic correlations.

In summary, the combined analyses of carbon isotopic and TOC data demonstrate that, despite the Ferrals-les-Montagnes section having undergone low-grade metamorphic conditions, the trends in the carbon isotopic signals remain reliable, enabling their use for chemostratigraphic purposes.

5.3. Series 2 – Miaolingian boundary and ROECE identification

The definition of the Series 2 – Miaolingian boundary is based on the FAD of the trilobite *Oryctocephalus indicus* (Peng et al., 2020). This species is not recorded from the western margin of Gondwana, where it is believed that the FAD of *O. indicus* correlates with a level in the upper part of the *Acadoparadoxides mureroensis* Biozone (Gozalo et al., 2013; Geyer, 2019). Furthermore, the usefulness of *O. indicus* as marker for the Stage 4 – Wuliuan boundary is a topic of ongoing debate (e.g., McCollum and Sundberg, 2005; Sundberg et al., 2020, 2022). In the Montagne Noire region, the Series 2 – Miaolingian boundary (Stage 4 – Wuliuan) is presumed to be situated between the lower part of PDP Formation and the top of LTQ Formation. In Ferrals-les-Montagnes, this interval is represented by a thickness of approximately 50 m where fossil preservation is poor, likely due to diagenesis (Álvaro and Vizcaïno, 1998; Álvaro et al., 2001a; Álvaro, 2020). Consequently, the precise location of the Stage 4 – Wuliuan boundary and the ROECE in Montagne Noire remain uncertain (Álvaro and Vizcaïno, 1998; Álvaro et al., 2001a; Álvaro, 2020). The biostratigraphic control provided in this study lends support to an early Drumian age for the base of the COU Formation. The results from previous studies (Wotte et al., 2007, 2012; Geyer, 2019; Álvaro, 2020) along with those from this investigation reduce the uncertainty regarding the location of the Stage 4 – Wuliuan boundary and the ROECE to 10 m (Fig. 3).

The ROECE is defined as a negative CIE around the Stage 4 – Wuliuan boundary, which corresponds roughly to the traditional lower-middle Cambrian boundary (Zhu et al., 2006; Álvaro, 2020; Peng et al., 2020). The negative excursion peak typically records $\delta^{13}C_{carb}$ values of −4 ‰, with a range from −1.3 ‰ in the Georgina Basin (Australia, North Gondwana, Donnelly et al., 1988) up to −15 ‰ on Tarim (Wu et al., 2021). Based on chemo- and biostratigraphic data, the ROECE is documented on Laurentia (Montañez et al., 2000; Dilliard et al., 2007; Wotte et al., 2011; Faggetter et al., 2016, 2019; Lin et al., 2019), South China (Zhu et al., 2004; Guo et al., 2010; Chang et al., 2017; Lin et al., 2019; Liu et al., 2021; Zhang et al., 2022), North China (Zhu et al., 2004; He et al., 2022; Zuo et al., 2023), Tarim (Wang et al., 2011; Guo et al., 2017; Wu et al., 2021), Siberia (Brasier and Sukhov, 1998; Shabanov et al., 2008; Wotte et al., 2011), northern Gondwana (Donnelly et al., 1988; Hall, 2012; Schmid, 2017; Birksmith et al., 2023), and potentially eastern Gondwana (Gomez et al., 2007; Gomez and Astini, 2015).

In Baltica, Avalonia, and western Gondwana, epeirogenic uplift and the associated shallowing-upward phase at the Stage 4 – Wuliuan boundary preclude precise resolution of this excursion. In Baltica, Fan et al. (2011) proposed a correlation between the negative excursion identified by Álvaro et al. (2010a) and the ROECE. However, the data points delineating this negative excursion are situated below and above an unconformity that spans the upper Stage 4 and lower Wuliuan Stage (see Álvaro et al., 2010a). This is at odds with the younger age (e.g., middle/late Wuliuan) of the ROECE proposed by Fan et al. (2011). In

Avalonia, the absence of upper Stage 4 to middle Wuliuan strata is attributed to the epeirogenic uplift that affected the region (Landing et al., 2022a, 2022b). In western Gondwana, the uplift associated with the Stage 4 – Wuliuan is less pronounced. This allowed for the deposition of a complete sedimentary record at a few localities, during this interval. While studies documenting this interval have primarily been conducted in Spain (Wotte et al., 2007, 2012; Gozalo et al., 2013) and southern France (Wotte et al., 2007, 2012), none have provided conclusive evidence for the presence of the ROECE. Gozalo et al. (2013) documented a −40 ‰ negative shift in $\delta^{13}C_{org}$, which is likely associated with ROECE, but interpretation should be approached with caution, given the unusually negative values for both the ROECE and the Cambrian in general (e.g., Fig. 6A).

In this study, as explained in section 5.b, the trend of the $\delta^{13}C$ data in the inferred ROECE interval are considered reliable, despite the low-grade metamorphism of the Ferrals-les-Montagnes section. We suggest that the matching negative excursions in $\delta^{13}C_{carb}$ and $\delta^{13}C_{org}$ correspond to the ROECE in the Ferrals-les-Montagnes section. Another line of evidence supporting our hypothesis is that these coeval excursions occur in a stratigraphic interval corresponding to the expected Stage 4 – Wuliuan boundary. When comparing the $\delta^{13}C_{carb}$ trends in the Ferrals-Les-Montagnes section with the GTS 2020 global curve for the ROECE – DICE interval (Peng et al., 2020) a similar pattern is observed corroborating the identification of these isotope excursions.

5.4. DICE identification

The Wuliuan – Drumian boundary is defined by the FAD of the agnostid *Ptychagnostus atavus* (Babcock et al., 2007; Peng et al., 2020). This species is not known from western Gondwana; however, it has been established that the FAD of *Pt. atavus* is roughly equivalent to the *Badulesia granieri/Pardailhania hispida* zonal boundary in Mediterranean subprovinces. In the Ferrals-les-Montagnes section, this level corresponds to the boundary between the LTQ and COU formations (e.g., Álvaro and Vizcaïno, 1998; Gozalo et al., 2011; Geyer, 2019).

The DICE is defined as a negative CIE located approximately at the base of the Drumian Stage (Zhu et al., 2006; Babcock et al., 2007; Peng et al., 2020). The excursion peak typically records $\delta^{13}C_{carb}$ values around −2 ‰, though it can vary from −1.5 ‰ in the Amadeus Basin (Australia, North Gondwana, Schmid, 2017) up to −4 ‰ in Siberia and eastern Laurentia (Shembilu and Azmy, 2021; Kouchinsky et al., 2022). Based on chemo- and biostratigraphic data, the DICE is located at approximately the Wuliuan – Drumian boundary in Laurentia (Montañez et al., 2000; Babcock et al., 2007; Howley and Jiang, 2010; Faggetter et al., 2016; Shembilu and Azmy, 2021), South China (Zhu et al., 2006; Li et al., 2020; Dong et al., 2025; Li et al., 2025), North China (Zhu et al., 2004; Zuo et al., 2023), Tarim (Wu et al., 2021; Yang et al., 2021), Siberia (Kouchinsky et al., 2022), North Gondwana (Pagès and Schmid, 2016; Schmid, 2017), and potentially East Gondwana (Gomez et al., 2007; Gomez and Astini, 2015).

In the southern Montagne Noire, Álvaro et al. (2008) made a first attempt to identify the DICE using $\delta^{13}C_{org}$. However, a comprehensive review of the literature, presented in the following four points, indicates that their negative excursion is unlikely to represent the DICE. (1) Following Álvaro et al. (2008), the negative excursion is situated within the middle Languedocian La Gardie Formation, which is of Guzhangian age (Geyer, 2019). Consequently, this formation is considerably younger than the base of the Drumian Stage, where the DICE is defined (Babcock et al., 2007; Peng et al., 2020). (2) The majority of the DICE reported in the literature are defined using $\delta^{13}C_{carb}$ values, which are not compared with the $\delta^{13}C_{org}$ values. It is tenuous to rely solely on the $\delta^{13}C_{org}$ to identify the DICE. (3) Álvaro et al. (2008) used TOC values from siliciclastic rocks to identify the DICE, but these values were exceptionally low, around 0.05 wt%, falling below the analytical threshold of 0.1 wt%. (4) The fossil assemblage reported in this study confirms that the Coulouma Formation is of Drumian age. Therefore, the La Gardie Formation, being two formations younger, cannot record the DICE.

In this study, as explained in section 5.b, the trend of the $\delta^{13}C$ data from the presumed DICE interval are considered reliable, despite the low-grade metamorphic conditions of the studied section. The biostratigraphic data available place the Wuliuan – Drumian boundary at the LTQ – COU formational boundary, in line with the data presented by Gozalo et al. (2011) and Geyer (2019). Although the precise identification of the DICE based on $\delta^{13}C_{carb}$ remains limited in the upper part of the section (due to the low carbonate content), our data, combined with those from Wotte et al. (2012), suggest a 1.5 ‰ $\delta^{13}C_{carb}$ negative excursion. This excursion coincides with the observed 1.3 ‰ $\delta^{13}C_{org}$ negative excursion. While the $\delta^{13}C_{org}$ isotope excursion is based on a limited number of samples, we suggest that the co-occurrence of both $\delta^{13}C_{carb}$ and $\delta^{13}C_{org}$ excursions near the presumed Wuliuan – Drumian boundary likely corresponds to the DICE (Fig. 3).

5.5. Correlation of western Gondwana with the global carbon isotope framework

Identification of the ROECE and the DICE at Ferrals-les-Montagnes allows us to compare western Gondwana with other localities. A comprehensive examination of the literature reveals 126 locations that document sedimentary successions spanning the lower-middle Cambrian interval, but only 9 of these sites document both the ROECE and the DICE concurrently (Fig. 7; details in Supplementary Materials 3). At seven of these sites, the Wuliuan Stage boundary has also been identified.

Whereas local factors may have overprinted the $\delta^{13}C$ records, data from these nine localities (excluding section 10, which does not record the ROECE), exhibit a consistent $\delta^{13}C_{carb}$ trend throughout the Stage 4 – lower Drumian interval. This trend can be divided into four distinct steps, which mirror the pattern observed in the Geological Time Scale carbon isotope framework: (1) Stage 4 is characterized by stable $\delta^{13}C_{carb}$ values around 0 ‰. (2) The Stage 4 – Wuliuan transition is marked by a negative excursion in $\delta^{13}C_{carb}$ (ROECE), which is followed by a rapid return to pre-excursion values of approximately 0 ‰. (3) Through the Wuliuan Stage, there is a noticeable gradual decrease in $\delta^{13}C_{carb}$ values until the top of the stage. (4) The Wuliuan – Drumian transition is marked by a negative $\delta^{13}C_{carb}$ excursion (DICE), succeeded by a swift return to pre-excursion values of about 0 ‰. Both the $\delta^{13}C_{carb}$ and 13 C_{org} curves align with this four-step pattern in the Ferrals-les-Montagnes section, allowing correlation of western Gondwana with the global carbon isotope framework.

In the Wangcun section (4), the onset of the ROECE excursion occurs below the Stage 4 – Wuliuan boundary. However, in the La Laja section (2), the ROECE is above the Stage 4 –Wuliuan boundary. This diachronism may be due to the shift from an endemic to a cosmopolitan-dominated communities during the Wuliuan Stage. This transition poses a significant challenge for the accurate biostratigraphic correlation of these localities. Furthermore, as noted in part 5c, this suggests that the FO of *O. indicus* may not be the most accurate marker for identifying the Stage 4 – Wuliuan boundary, especially when compared to the ROECE, which is thought to be a global and synchronous phenomenon.

In the case of the DICE, offsets are observed between the excursion minimum and the FO of *P. atavus* (or equivalent) in the La Laja section (2), Dingo 2 well (3), Shatan section (5), Xiaoerbulak section (6), and Molodo River section (7); suggesting a limited asynchrony or incorrect positioning of *P. atavus* compared to the DICE.

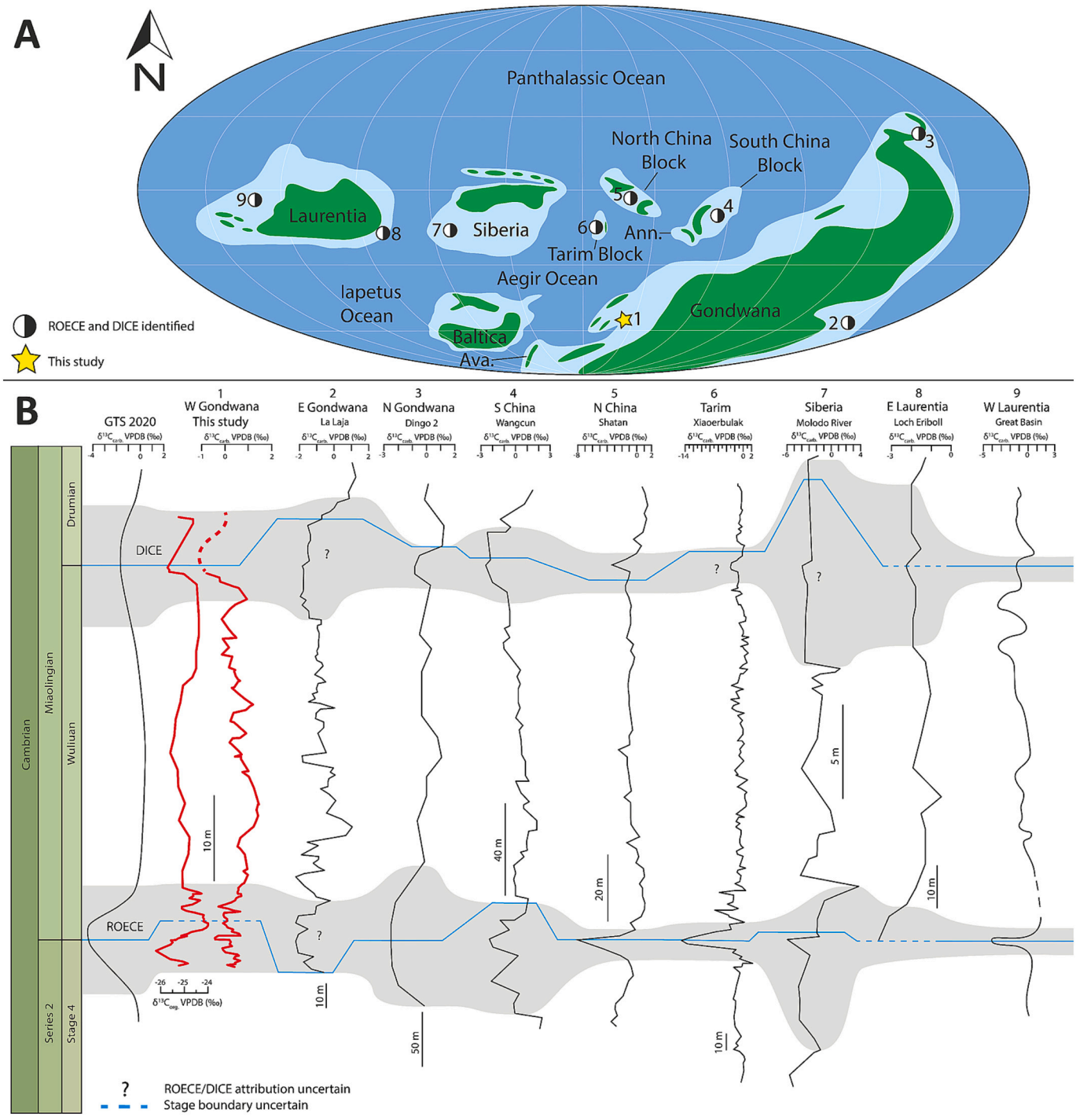

Fig. 7. Correlation of the Ferrals-les-Montagnes section (W Gondwana) with the global carbon geochemical framework. A – Localities recording the ROECE and the DICE on different paleocontinents. B – $\delta^{13}C$ isotope curves from Peng et al. (2020), this study (1), La Laja section (2) from Gomez and Astini (2015), Dingo 2 well (3) from Schmid (2017), Wangcun section (4) from Zhu et al. (2004), Shatan section (5) from Zuo et al. (2023), Xiaoerbulak section (6) from Wu et al. (2021), Molodo River section (7) from Shabanov et al. (2008), Loch Eriboll section (8) from Faggetter et al. (2016), and Great Basin composite section (9) from Montañez et al. (2000). The gray shaded areas correspond to the ROECE and DICE intervals. For identification of the ROECE and DICE in the different section, see Supplementary Materials 2. For a complete list of the localities that recorded the Stage 4 – Drumian interval, see Supplementary Materials 3. Abbreviations: Ann. – Annamia, Ava. – Avalonia.

6. Conclusions

The Ferrals-les-Montagnes section in southern France provides a high-resolution record of the middle – late Cambrian in the Montagne Noire area, which represents one of the most complete outer-ramp and deep-shelf records of this period described from western Gondwana. Analyses of $\delta^{13}C_{carb}$ and $\delta^{13}C_{org}$ datasets reveal two negative excursions, which are attributed to the ROECE and the DICE events. Recognition of these events together with newly collected fossils increases our confidence in the stratigraphic position of the Stage 4 – Wuliuan and Wuliuan – Drumian boundaries in the Ferrals-les-Montagnes section and thus provides a better understanding of the Series 2 – Miaolingian transition

in western Gondwana. Despite diagenetic and metamorphic overprints, carbon isotope geochemistry, Rock-Eval data, and thin-section analyses confirm the preservation of the ROECE and DICE. The Ferrals-les-Montagnes $\delta^{13}C$ profile aligns with global records and the GTS 2020 curve, placing it as a key reference to increase our understanding of the Cambrian in western Gondwana.

CRediT authorship contribution statement

Valentin Jamart: Writing – original draft, Visualization, Formal analysis, Conceptualization. **Damien Pas:** Writing – review & editing, Supervision, Funding acquisition, Conceptualization. **Thierry Adatte:** Writing – review & editing. **Jorge E. Spangenberg:** Writing – review & editing. **Lukáš Laibl:** Writing – review & editing. **Allison C. Daley:** Writing – review & editing.

Declaration of competing interest

The authors declare that they have no known competing financial interests or personal relationships that could have appeared to influence the work reported in this paper.

Data availability

Data will be made available on request.

Acknowledgments

This work is supported by an Ambizione fellowship awarded by the Swiss National Science Foundation to Damien Pas (grant n°193520). Work of Lukáš Laibl was conducted within institutional support RVO 67985831 of the Institute of Geology of the Czech Academy of Sciences. We are grateful to Mr. Eric Monceret and Prof. Bertrand Lefebvre for their help in echinoderm identification and the access to old historical papers related to the Montagne Noire. Finally, we gratefully thank the editor Dr. Bing Shen and the two reviewers Prof. Jih-Pai Lin and the anonymous reviewer for their time and all the constructive comments that improved this contribution.

Appendix A. Supplementary data

Supplementary data to this article can be found online at https://doi.org/10.1016/j.palaeo.2025.112951.

References

Advanced Analytical Center, J. C. U., Australia. Element-to-stoichiometric oxide conversion factors. Retrieved 19th of August 2024 from. https://www.jcu.edu.au/advanced-analytical-centre/resources/element-to-stoichiometric-oxide-conversion-factors.

Álvaro, J.J., 2020. Calibrating δ13C and δ18O chemostratigraphic correlations across Cambrian strata of SW Europe and Morocco, West Gondwana. In: Montenari, M. (Ed.), Carbon Isotope Stratigraphy, vol. 5. Elsevier, pp. 269–317. https://doi.org/10.1016/bs.sats.2020.08.003.

Álvaro, J.J., Clausen, S., 2005. Major geodynamic and sedimentary constraints on the chronostratigraphic correlation of the lower-middle Cambrian transition in the western Mediterranean region. Geosci. J. 9 (2), 145–160. https://doi.org/10.1007/Bf02910576.

Álvaro, J.J., Vennin, E., 1996. Tectonic control on Cambrian sedimentation in South-Western Europe. Eclogae Geol. Helv. 89 (3), 935–948.

Álvaro, J.J., Vennin, E., 1998. Stratigraphic signature of a terminal early Cambrian regressive event in the Iberian Peninsula. Can. J. Earth Sci. 35 (4), 402–411.

Álvaro, J.J., Vizcaïno, D., 1997. Révision des trilobites Solenopleuropsinae du Cambrien Moyen de la Montagne Noire (France). Geobios 30 (4), 541–561. https://doi.org/10.1016/S0016-6995(97)80121-0.

Álvaro, J.J., Vizcaïno, D., 1998. Révision biostratigraphique du Cambrien moyen du versant méridional de la Montagne Noire (Languedoc, France). Bulletin de la Société géologique de France 169 (2), 233–242.

Álvaro, J.J., Vizcaïno, D., 2000. Nouvel assemblage de trilobites dans le Cambrien moyen de la nappe de Pardaihlan (Montagne Noire, France) : implications biostratigraphiques dans la région méditerranéenne. Eclogae Geol. Helv. 93 (3), 277–289.

Álvaro, J.J., Vizcaïno, D., 2001. The southern Montagne Noire: a key region for the research on lower Paleozoic paleontology. Annales de la Société géologique du Nord 8 (4), 185–189.

Álvaro, J.J., Coujault-Radé, P., Chauvel, J.J., Dabard, M.P., Debrenne, F., Feist, R., Pillola, G.L., Vennin, E., Vizcaïno, D., 1998. Nouveau découpage stratigraphique des séries cambriennes des nappes de Pardaihlan et du Minervois (versant sud de la Montagne Noire). Géol. Fr. 2, 3–12.

Álvaro, J.J., Vizcaïno, D., Vennin, E., 1999. Trilobite diversity patterns in the Middle Cambrian of southwestern Europe: a comparative study. Palaeogeogr. Palaeoclimatol. Palaeoecol. 151 (4), 241–254. https://doi.org/10.1016/S0031-0182(99)00033-4.

Álvaro, J.J., Vennin, E., Moreno-Eiris, E., Perejon, A., Bechstadt, T., 2000. Sedimentary patterns across the Lower-Middle Cambrian transition in the Esla nappe (Cantabrian Mountains, northern Spain). Sediment. Geol. 137 (1–2), 43–61. https://doi.org/10.1016/S0037-0738(00)00134-2.

Álvaro, J.J., Debrenne, F., Vizcaïno, D., 2001a. The lower Cambrian of the southern Montagne Noire. Annales de la Société géologique du Nord 8 (4), 201–204.

Álvaro, J.J., Lefebvre, B., Shergold, J.H., Vizcaïno, D., 2001b. The middle-upper Cambrian of the southern Montagne Noire. Annales de la Société géologique du Nord 8 (4), 205–211.

Álvaro, J.J., Elicki, O., Geyer, G., Rushton, A.W.A., Shergold, J.H., 2003. Palaeogeographical controls on the Cambrian trilobite immigration and evolutionary patterns reported in the western Gondwana margin. Palaeogeogr. Palaeoclimatol. Palaeoecol. 195 (1–2), 5–35. https://doi.org/10.1016/S0031-0182(03)00300-6.

Álvaro, J.J., Vizcaïno, D., Kordule, V., Fatka, O., Pillola, G.L., 2004. Some solenopleurine trilobites from the Languedocian (late Mid Cambrian) of western Europe. Geobios 37 (2), 135–147.

Álvaro, J.J., Bauluz, B., Subias, I., Pierre, C., Vizcaïno, D., 2008. Carbon chemostratigraphy of the Cambrian-Ordovician transition in a midlatitude mixed platform, Montagne Noire France. Geol. Soc. Am. Bull. 120 (7–8), 962–975. https://doi.org/10.1130/B26243.1.

Álvaro, J.J., Ahlberg, P., Axheimer, N., 2010a. Skeletal carbonate productivity and phosphogenesis at the lower-middle Cambrian transition of Scania, southern Sweden. Geol. Mag. 147 (1), 59–76. https://doi.org/10.1017/S0016756809990021.

Álvaro, J.J., Monceret, E., Monceret, S., Verraes, G., Vizcaïno, D., 2010b. Stratigraphic record and palaeogeographic context of the Cambrian Epoch 2 subtropical carbonate platforms and their basinal counterparts in SW Europe West Gondwana. Bull. Geosci. 85 (4), 573–584. https://doi.org/10.3140/bull.geosci.1179.

Álvaro, J.J., Zamora, S., Clausen, S., Vizcaïno, D., Smith, A.B., 2013. The role of abiotic factors in the Cambrian Substrate Revolution: a review from the benthic community replacements of West Gondwana. Earth Sci. Rev. 118, 69–82. https://doi.org/10.1016/j.earscirev.2013.01.002.

Álvaro, J.J., Bauluz, B., Clausen, S., Devaere, L., Imaz, A.G., Monceret, E., Vizcaïno, D., 2014. Stratigraphic review of the Cambrian-lower Ordovician volcanosedimentary complexes from the northern Montagne Noire France. Stratigraphy 11 (1), 83–96.

Álvaro, J.J., Casas, J.M., Quesada, C., 2020. Reconstructing the pre-Variscan puzzle of Cambro-Ordovician basement rocks in the southwestern European margin of Gondwana. Pannotia to Pangaea: Neoproterozoic and Paleozoic Orogenic Cycles in the Circum-Atlantic Region 503, 531–562. https://doi.org/10.1144/Sp503-2020-89.

Angelin, N.P., 1854. Palaeontologia Scandinavica. Pars I. Crustacea Formationis Transitionis. In: *Fasc. II.* Academiae Regiae Scientiarum Suecanae. T.O. Weigel, Lipsia (=Leipzig) i–ix + 21–92.

Babcock, L.E., Robison, R.A., Rees, M.N., Peng, S.-C., Saltzman, M.R., 2007. The global boundary stratotype section and point (GSSP) of the Drumian stage (Cambrian) in the drum mountains, Utah, USA. Episodes 30 (2), 85–95. https://doi.org/10.18814/epiiugs/2007/v30i2/003.

Babcock, L.E., Peng, S.-C., Brett, C.E., Zhu, M.-Y., Ahlberg, P., Bevis, M., Robison, R.A., 2015. Global climate, sea level cycles, and biotic events in the Cambrian Period. Palaeoworld 24 (1–2), 5–15. https://doi.org/10.1016/j.palwor.2015.03.005.

Behar, F., Beaumont, V., Penteado, H.L.D.B., 2001. Rock-Eval 6 technology: Performances and developments. Oil & Gas Science and Technology-Revue D Ifp Energies Nouvelles 56 (2), 111–134. https://doi.org/10.2516/ogst:2001013.

Birksmith, C., Brock, G.A., Betts, M.J., Holmes, J.D., Zhang, Z., 2023. Chronostratigraphy of the Cambrian Series 2 – Miaolingian boundary, western Stansbury Basin, South Australia. In: Paleo Down Under 3 - Abstract Book & Conference Guide.

Bottjer, D.J., Hagadorn, J.W., Dornbos, S.Q., 2000. The Cambrian Substrate Revolution. GSA Today 10 (9), 2–7.

Brand, W.A., Coplen, T.B., Vogl, J., Rosner, M., Prohaska, T., 2014. Assessment of international reference materials for isotope-ratio analysis (IUPAC Technical Report). Pure Appl. Chem. 86 (3), 425–467. https://doi.org/10.1515/pac-2013-1023.

Brasier, M.D., 1996. The Basal Cambrian transition and Cambrian Bio-events (from Terminal Proterozoic Extinctions to Cambrian Biomeres). In: Walliser, O.H. (Ed.), Global Events and Events Stratigraphy in the Phanerozoic. Springer-Verlag, pp. 113–138. https://doi.org/10.1007/978-3-642-79634-0.

Brasier, M.D., Sukhov, S.S., 1998. The falling amplitude of carbon isotopic oscillations through the lower to middle Cambrian: northern Siberia data. Can. J. Earth Sci. 35 (4), 353–373. https://doi.org/10.1139/e97-122.

Briggs, D.E.G., 2015. The Cambrian explosion. Curr. Biol. 25 (19), R864–R868. https://doi.org/10.1016/j.cub.2015.04.047.

Buatois, L.A., Almond, J., Mangano, M.G., Jensen, S., Germs, G.J.B., 2018. Sediment disturbance by Ediacaran bulldozers and the roots of the Cambrian explosion. Sci. Rep. 8. https://doi.org/10.1038/s41598-018-22859-9.

Cabibel, J., Termier, H., Termier, G., 1959. Les echinoderms mesocambriens de la Montagne Noire. Annales de Paleontologie 44, 281–294.

Chang, C., Hu, W., Wang, X., Yu, H., Yang, A., Cao, J., Yao, S., 2017. Carbon isotope stratigraphy of the lower to middle Cambrian on the eastern Yangtze Platform, South China. Palaeogeogr. Palaeoclimatol. Palaeoecol. 479, 90–101. https://doi.org/10.1016/j.palaeo.2017.04.019.

Cocks, L.R.M., 2000. The early Palaeozoic geography of Europe. J. Geol. Soc. Lond. 157 (1), 1–10.

Cohen, K.M., Finney, S.C., Gibbard, P.L., Fan, J.X., 2013. The ICS International Chronostratigraphic Chart. Episodes 36 (3), 199–204. https://doi.org/10.18814/epiiugs/2013/v36i3/002.

Courtessole, R., 1973. Le Cambrien Moyen de la Montagne Noire. Publié avec le concours du Laboratoire de Géologie CEARN de la Faculté des Sciences de Toulouse.

Cramer, B.D., Jarvis, I., 2020. Carbon Isotope Stratigraphy. In: Gradstein, F.M., Ogg, J.G., Schmitz, M.D., Ogg, G.M. (Eds.), Geological Time Scale 2020, vol. 2. Elsevier, pp. 309–343. https://doi.org/10.1016/B978-0-12-824360-2.00011-5.

Da Silva, A.C., Triantafyllou, A., Delmelle, N., 2023. Portable x-ray fluorescence calibrations: Workflow and guidelines for optimizing the analysis of geological samples. Chem. Geol. 623. https://doi.org/10.1016/j.chemgeo.2023.121395.

Demange, M., 2001. Tectono-stratigraphic setting of the southern slope nappes of Montagne Noire. Annales de la Société géologique du Nord 8 (4), 191–200.

Devaere, L., Clausen, S., Steiner, M., Álvaro, J.J., Vachard, D., 2013. Chronostratigraphic and palaeogeographic significance of an early Cambrian microfauna from the Heraultia Limestone, northern Montagne Noire, France. Palaeontol. Electron. 16 (2).

Dilliard, K.A., Pope, M.C., Coniglio, M., Hasiotis, S.T., Lieberman, B.S., 2007. Stable isotope geochemistry of the lower Cambrian Sekwi Formation, Northwest Territories, Canada: Implications for ocean chemistry and secular curve generation. Palaeogeogr. Palaeoclimatol. Palaeoecol. 256 (3–4), 174–194. https://doi.org/10.1016/j.palaeo.2007.02.031.

Dong, Y.X., Wang, J.Y., Zhong, Y.J., Chen, A.Q., Zheng, R.T., Zhu, P., Zhang, C., Han, Z., Cui, Y., 2025. The paleoenvironmental evolution of the Cambrian Miaolingian Epoch in South China. Palaeogeogr. Palaeoclimatol. Palaeoecol. 661. https://doi.org/10.1016/j.palaeo.2024.112713.

Donnelly, T.H., Shergold, J.H., Southgate, P.N., 1988. Anomalous Geochemical Signals from Phosphatic Middle Cambrian Rocks in the Southern Georgina Basin Australia. Sedimentology 35 (4), 549–570. https://doi.org/10.1111/j.1365-3091.1988.tb01235.x.

Espitalié, J., Deroo, G., Marquis, F., 1985. La pyrolyse Rock-Eval et ses applications. Deuxième partie. Revue de l'Institut Français du Pétrole 40 (6), 755–784. https://doi.org/10.2516/ogst:1985045.

Faggetter, L.E., Wignall, P.B., Pruss, S.B., Sun, Y.D., Raine, R.J., Newton, R.J., Widdowson, M., Joachimski, M.M., Smith, P.M., 2016. Sequence stratigraphy, chemostratigraphy and facies analysis of Cambrian Series 2-Series 3 boundary strata in northwestern Scotland. Geol. Mag. 155 (4), 865–877. https://doi.org/10.1017/S0016756816000947.

Faggetter, L.E., Wignall, P.B., Pruss, S.B., Jones, D.S., Grasby, S., Widdowson, M., Newton, R.J., 2019. Mercury chemostratigraphy across the Cambrian Series 2-Series 3 boundary: evidence for increased volcanic activity coincident with extinction? Chem. Geol. 510, 188–199. https://doi.org/10.1016/j.chemgeo.2019.02.006.

Fan, R., Deng, S.H., Zhang, X.L., 2011. Significant carbon isotope excursions in the Cambrian and their implications for global correlations. Sci. China-Earth Sci. 54 (11), 1686–1695. https://doi.org/10.1007/s11430-011-4313-z.

Friedrich, W.P., 1993. Systematik und Funktionsmorphologie mittelkambrischer Cincta (Carpoidea, Echinodermata). Beringeria 7, 3–190.

Geyer, G., 2019. A comprehensive Cambrian correlation chart. Episodes 42 (4), 321–332. https://doi.org/10.18814/epiiugs/2019/019026.

Gèze, B., 1949. Etude géologique de la Montagne Noire et des Cévennes méridionales. Société Géologique de France.

Gomez, F.J., Astini, R.A., 2015. Sedimentology and sequence stratigraphy from a mixed (carbonate-siliciclastic) rift to passive margin transition: the early to Middle Cambrian of the argentine Precordillera. Sediment. Geol. 316, 39–61. https://doi.org/10.1016/j.sedgeo.2014.11.003.

Gomez, F.J., Ogle, N., Astin, R.A., Kalin, R.M., 2007. Paleoenvironmental and carbon-oxygen isotope record of middle Cambrian carbonates (la Laja formation) in the argentine precordillera. J. Sediment. Res. 77 (9–10), 826–842. https://doi.org/10.2110/jsr.2007.079.

Gozalo, R., Liñán, E., Dies Álvarez, M.E., Gámez Vintaned, J.A., Mayoral, E., 2007. The Lower-Middle Cambrian boundary in the Mediterranean subprovince. Evolution of the Rheic Ocean: From Avalonian-Cadomian Active Margin to Alleghenian-Variscan Collision 423, 359–373. https://doi.org/10.1130/2007.2423(17).

Gozalo, R., Chirivella Martorell, J.B., Esteve, J., Liñán, E., 2011. Correlation between the base of Drumian Stage and the base of middle Caesaraugustan Stage in the Iberian chains (NE Spain). Bull. Geosci. 86 (3), 545–554. https://doi.org/10.3140/bull.geosci.1254.

Gozalo, R., Alvarez, M.E.D., Gámez Vintaned, J.A., Zhuravlev, A.Y., Bauluz, B., Subias, I., Chirivella Martorell, J.B., Mayoral, E., Gursky, H.J., Andres, J.A., Liñán, E., 2013. Proposal of a reference section and point for the Cambrian Series 2-3 boundary in the Mediterranean subprovince in Murero (NE Spain) and its intercontinental correlation. Geol. J. 48 (2–3), 142–155. https://doi.org/10.1002/gj.1330.

Guo, Q.J., Strauss, H., Liu, C.Q., Zhao, Y.L., Yang, X.L., Peng, J., Yang, H., 2010. A negative carbon isotope excursion defines the boundary from Cambrian Series 2 to Cambrian Series 3 on the Yangtze Platform, South China (vol 285, pg 143, 2010). Palaeogeogr. Palaeoclimatol. Palaeoecol. 288 (1–4), 118. https://doi.org/10.1016/j.palaeo.2010.01.022.

Guo, Q.J., Deng, Y.N., Hu, J., Wang, L.Y., 2017. Carbonate carbon isotope evolution of seawater across the Ediacaran-Cambrian transition: evidence from the Keping area, Tarim Basin NW China. Geol. Mag. 154 (6), 1244–1256. https://doi.org/10.1017/S0016756817000206.

Hall, P.A., 2012. Elemental, isotopic and molecular signatures of early Cambrian marine sediments and a phantom petroleum system in South Australia. University of Adelaide. https://hdl.handle.net/2440/81757.

Hawle, I., Corda, A.J.C., 1847. Prodrom einer Monographie der bohmischen Trilobiten. Abhandlungen der königlichen böhmischen Gesellschaft der Wissenschaften 5, 119–292.

He, W.Y., Qi, Y.A., Dai, M.Y., Liu, B.C., Li, J.B., Xu, G.X., Wang, M., Li, D., 2022. Facies changes, Evolution of Biogenic Structures, and Carbon Isotope Stratigraphy of the Cambrian Series 2 to Miaolingian transition on the Southern North China Craton. Minerals 12 (12). https://doi.org/10.3390/min12121526.

Hoefs, J., 2021. Stable Isotope Geochemistry, 9th ed. Springer International Publishing : Imprint: Springer. https://doi.org/10.1007/978-3-030-77692-3.

Hough, M.L., Shields, G.A., Evins, L.Z., Strauss, H., Henderson, R.A., Mackenzie, S., 2006. A major Sulphur isotope event at c.510 Ma: a possible anoxia-extinction-volcanism connection during the Early-Middle Cambrian transition? Terra Nova 18 (4), 257–263. https://doi.org/10.1111/j.1365-3121.2006.00687.x.

Howley, R.A., Jiang, G., 2010. The Cambrian Drumian carbon isotope excursion (DICE) in the Great Basin, western United States. Palaeogeogr. Palaeoclimatol. Palaeoecol. 296 (1–2), 138–150. https://doi.org/10.1016/j.palaeo.2010.07.001.

Irwin, H., Curtis, C., Coleman, M., 1977. Isotopic evidence for source of Diagenetic Carbonates formed during Burial of Organic-Rich Sediments. Nature 269 (5625), 209–213. https://doi.org/10.1038/269209a0.

Jaekel, O., 1918. Phylogenie und System der Pelmatozoen. Paläontol. Z. 3, 1–128.

Jourdan, F., Hodges, K., Sell, B., Schaltegger, U., Wingate, M.T.D., Evins, L.Z., Soderlund, U., Haines, P.W., Phillips, D., Blenkinsop, T., 2014. High-precision dating of the Kalkarindji large igneous province, Australia, and synchrony with the Early-Middle Cambrian (stage 4-5) extinction. Geology 42 (6), 543–546. https://doi.org/10.1130/G35434.1.

Kaufman, A.J., Knoll, A.H., 1995. Neoproterozoic Variations in the C-Isotopic Composition of Seawater - Stratigraphic and Biogeochemical Implications. Precambrian Res. 73 (1–4), 27–49. https://doi.org/10.1016/0301-9268(94)00070-8.

Kouchinsky, A., Alexander, R., Bengtson, S., Bowyer, F., Clausen, S., Holmer, L.E., Kolesnikov, K.A., Korovnikov, I.V., Pavlov, V., Skovsted, C.B., Ushatinskaya, G., Wood, R., Zhuravlev, A.Y., 2022. Early-middle Cambrian stratigraphy and faunas from northern Siberia. Acta Palaeontol. Pol. 67 (2), 341–464. https://doi.org/10.4202/app.00930.2021.

Krissansen-Totton, J., Buick, R., Catling, D.C., 2015. A Statistical Analysis of the Carbon Isotope Record from the Archean to Phanerozoic and Implications for the rise of Oxygen. Am. J. Sci. 315 (4), 275–316. https://doi.org/10.2475/04.2015.01.

Landing, E., Westrop, S.R., Geyer, G., 2022a. Trans-Avalonian green-black boundary (early Middle Cambrian): transform fault-driven epeirogeny and onset of 26 m.y. of shallow-marine, black mudstone in Avalonia (Rhode Island-Belgium) and Baltica. Can. J. Earth Sci. https://doi.org/10.1139/cjes-2022-0065.

Landing, E., Keppie, J.D., Keppie, D.F., Geyer, G., Westrop, S.R., 2022b. Greater Avalonia-latest Ediacaran-Ordovician "peribaltic " terrane bounded by continental margin prisms ("Ganderia, " Harlech Dome, Meguma): Review, tectonic implications, and paleogeography. Earth Sci. Rev. 224. https://doi.org/10.1016/j.earscirev.2021.103863.

Landing, E., Webster, M., Bowser, S.S., 2023. Terminal Ediacaran-late Ordovician evolution of the NE Laurentia palaeocontinent: rift-drift-onset of Taconic Orogeny, sea-level change and 'Hawke Bay' onlap (not offlap). Geol. Soc. Lond. Spec. Publ. 542. https://doi.org/10.1144/sp542-2023-4.

Li, D., Zhang, X., Zhang, X., Zhu, H., Peng, S.-C., Sun, L., Shen, Y., 2020. A paired carbonate-organic δ13C approach to understanding the Cambrian Drumian carbon isotope excursion (DICE). Precambrian Res. 349. https://doi.org/10.1016/j.precamres.2019.105503.

Li, Z., Yang, X.L., Yuan, Y., Hu, Y., Wang, D.Z., 2025. Carbon isotope fluctuations from the Cambrian Jialao Formation in Jianhe County, Guizhou Province, China: Implications for stratigraphic correlation. Palaeogeogr. Palaeoclimatol. Palaeoecol. 661. https://doi.org/10.1016/j.palaeo.2024.112680.

Lin, J.-P., Sundberg, F.A., Jiang, G., Montañez, I.P., Wotte, T., 2019. Chemostratigraphic correlations across the first major trilobite extinction and faunal turnovers between Laurentia and South China. Sci. Rep. 9. https://doi.org/10.1038/s41598-019-53685-2.

Liu, Z.R.R., Zhou, M.F., Chen, W.T., Williams-Jones, A.E., Li, X.D., Yin, R.S., O'Brien, H., Lahaye, Y., 2021. Mercury and sulfur isotopic evidence for the linkages between the ca. 510 Ma Kalkarindji large igneous province and trilobite crisis. Earth Planet. Sci. Lett. 566. https://doi.org/10.1016/j.epsl.2021.116947.

Mangano, M.G., Buatois, L.A., 2017. The Cambrian revolutions: Trace-fossil record, timing, links and geobiological impact. Earth Sci. Rev. 173, 96–108. https://doi.org/10.1016/j.earscirev.2017.08.009.

McCollum, L.B., Sundberg, F.A., 2005. The use of *Oryctocephalus indicus* as a "Lower-Middle" Cambrian boundary GSSP: a status report. Acta Micropalaeontologica Sinica 22, 113–114.

Mckerrow, W.S., Scotese, C.R., Brasier, M.D., 1992. Early Cambrian Continental Reconstructions. J. Geol. Soc. Lond. 149, 599–606. https://doi.org/10.1144/gsjgs.149.4.0599.

Miquel, J., 1905. Essai sur le Cambrien de la Montagne Noire. Coulouma. L'Acadien. Bulletin de la Société géologique de France 5, 465–483.

Montañez, I.P., Osleger, D.A., Banner, J.L., Mack, L.E., Musgrove, M., 2000. Evolution of the Sr and C Isotope Composition of Cambrian Oceans. GSA Today 10 (5), 7.

Montmartin, C., Faure, M., Raimbourg, H., 2021. Paleotemperature investigation of the Variscan southern external domain: the case of the Montagne Noire (France). Bsgf-Earth Sci. Bull. 192. https://doi.org/10.1051/bsgf/2020043.

Munier-Chalmas, E., Bergeron, J., 1889. Etude du massif ancien situé au fond du plateau central. In: Bergeron, J. (Ed.), Annales de la Société Géologique, XXII, p. 338.
Nielsen, A.T., Schovsbo, N.H., 2015. The regressive Early-Mid Cambrian 'Hawke Bay Event' in Baltoscandia: Epeirogenic uplift in concert with eustasy. Earth Sci. Rev. 151, 288–350. https://doi.org/10.1016/j.earscirev.2015.09.012.
Pagès, A., Schmid, S., 2016. Euxinia linked to the Cambrian Drumian carbon isotope excursion (DICE) in Australia: Geochemical and chemostratigraphic evidence. Palaeogeogr. Palaeoclimatol. Palaeoecol. 461, 65–76. https://doi.org/10.1016/j.palaeo.2016.08.008.
Palmer, A.R., James, N.P., 1980. The Hawke Bay event: A circum-Iapetus regression near the Lower-Middle Cambrian boundary. In: Wones, D.R. (Ed.), The Caledonides in the USA, vol. 2. Department of Geological Sciences, Virginia Polytechnic Institue and State University Memoirs, pp. 15–18.
Peng, S.-C., Babcock, L.E., Ahlberg, P., 2020. The Cambrian Period. In: Gradstein, F.M., Ogg, J.G., Schmitz, M.D., Ogg, G.M. (Eds.), Geological Time Scale 2020, vol. 2. Elsevier, pp. 565–629. https://doi.org/10.1016/B978-0-12-824360-2.00019-X.
Peters, K.E., 1986. Guidelines for evaluating Petroleum Source Rock using Programmed Pyrolysis. AAPG Bull. Am. Assoc. Pet. Geol. 70 (3), 318–329.
Pompeckj, J.F., 1901. Versteinerungen der Paradoxides-Stufe von La Cabitza in Sardinien und Bemerkungen zur Gliederung des sardischen Cambrium. Z. Dtsch. Geol. Ges. 53, 1–23.
Potin, G.J.M., Daley, A.C., 2023. The significance of Anomalocaris and other Radiodonta for understanding paleoecology and evolution during the Cambrian explosion. Front. Earth Sci. 11, 1–26. https://doi.org/10.3389/feart.2023.1160285.
Potin, G.J.M., Gueriau, P., Daley, A.C., 2023. Radiodont frontal appendages from the Fezouata Biota (Morocco) reveal high diversity and ecological adaptations to suspension-feeding during the early Ordovician. Front. Ecol. Evol. 11, 1–22. https://doi.org/10.3389/feart.2023.1160285.
Raiswell, R., Berner, R.A., 1987. Organic carbon losses during burial and thermal maturation of normal marine shales. Geology 15 (9), 853–856. https://doi.org/10.1130/0091-7613(1987)15<853:Ocldba>2.0.Co;2.
Runnegar, B., 1982. The Cambrian Explosion - animals or Fossils. J. Geol. Soc. Aust. 29 (3–4), 395–411. https://doi.org/10.1080/00167618208729222.
Saleh, F., Antcliffe, J.B., Lustri, L., Daley, A.C., Gibert, C., 2023. Cambrian and Ordovician diversity fluctuations could be resolved through a single ecological hypothesis. Lethaia 56 (3), 1–13. https://doi.org/10.18261/let.56.3.7.
Schmid, S., 2017. Chemostratigraphy and palaeo-environmental characterisation of the Cambrian stratigraphy in the Amadeus Basin, Australia. Chem. Geol. 451, 169–182. https://doi.org/10.1016/j.chemgeo.2017.01.019.
Scotese, C.R., 2014. Atlas of Cambrian and Early Ordovician Paleogeographic Maps (Mollweide Projection), Maps 81–88, Volumes 5, The Early Paleozoic, PALEOMAP Atlas for ArcGIS, PALEOMAP Project, Evanston, IL.
Scotese, C.R., 2016. PALEOMAP Paleoatlas for GPlates and the PaleoData Plotter Program. PALEOMAP Project. 1–59. http://www.earthbyte.org/paleomap-paleoatlas-for-gplates.
Scotese, C.R., 2021. An Atlas of Phanerozoic Paleogeographic Maps: the Seas come in and the Seas Go out. Annu. Rev. Earth Planet. Sci. 49, 679. https://doi.org/10.1146/annurev-earth-081320-064052.
Sdzuy, K., Liñán, E., Gozalo, R., 1999. The Leonian stage (early Middle Cambrian): a unit for Cambrian correlation in the Mediterranean subprovince. Geol. Mag. 136 (1), 39–48. https://doi.org/10.1017/S0016756899002241.
Seilacher, A., 1999. Biomat-related lifestyles in the precambrian. Palaios 14 (1), 86–93. https://doi.org/10.2307/3515363.
Servais, T., Lehnert, O., Li, J., Mullins, G.L., Munnecke, A., Nützel, A., Vecoli, M., 2008. The Ordovician Biodiversification:: revolution in the oceanic trophic chain. Lethaia 41 (2), 99–109. https://doi.org/10.1111/j.1502-3931.2008.00115.x.
Servais, T., Perrier, V., Danelian, T., Klug, C., Martin, R., Munnecke, A., Nowak, H., Nützel, A., Vandenbroucke, T.R.A., Williams, M., Rasmussen, C.M.O., 2016. The onset of the 'Ordovician Plankton Revolution' in the late Cambrian. Palaeogeogr. Palaeoclimatol. Palaeoecol. 458, 12–28. https://doi.org/10.1016/j.palaeo.2015.11.003.
Shabanov, Y.Y., Korovnikov, I.V., Pereladov, V.S., Pak, K.L., Feflov, A.F., 2008. *The section of the Kuonamka Formation of the Molodo River - a candidate for a global stratigraphy of the lower boundary of the Middle Cambrian (East Siberian Platform)* Cambrian sections of the Siberian Platform—stratotype candidates for an international stratigraphic scaling (Stratigraphy and Palaeontology). In: Material of the 13th International Field Conference of the Cambrian Subdivision Working Group, Yakutia.
Sharp, Z., 2017. Principles of stable isotope geochemistry, 2nd ed. University of New Mexico. https://doi.org/10.25844/h9q1-0p82.
Shembilu, N., Azmy, K., 2021. Carbon-isotope stratigraphy of the Middle-Upper Cambrian in eastern Laurentia: Implications for global correlation. Mar. Pet. Geol. 128. https://doi.org/10.1016/j.marpetgeo.2021.105052.
Shergold, J.H., Feist, R., Vizcaïno, D., 2000. Early late Cambrian trilobites of Australo-Sinian aspect from the Montagne Noire, southern France. Palaeontology 43, 599–632. https://doi.org/10.1111/1475-4983.00142.
Smith, A.B., Zamora, S., 2009. Rooting Phylogenies of Problematic Fossil Taxa; a Case Study using Cinctans (Stem-Group Echinoderms). Palaeontology 52, 803–821. https://doi.org/10.1111/j.1475-4983.2009.00880.x.
Spangenberg, J.E., 2024. Three combustion reactions in a single elemental analysis and isotope ratio mass spectrometry acquisition as a strategy to save helium and energy. Rapid Commun. Mass Spectrom. 38 (1). https://doi.org/10.1002/rcm.9663.
Spangenberg, J.E., Herlec, U., 2006. Hydrocarbon biomarkers in the Topla-Mezica zinc-lead deposits, northern Karavanke/Drau Range, Slovenia: Paleoenvironment at the site of ore formation. Econ. Geol. 101 (5), 997–1021. https://doi.org/10.2113/gsecongeo.101.5.997.
Sundberg, F.A., Geyer, G., Kruse, P.D., McCollum, L.B., Pegel', T.V., Zylinska, A., Zhuravlev, A.Y., 2016. International correlation of the Cambrian Series 2-3, Stages 4-5 boundary interval. Cambro-Ordovician Studies Vi 49, 83–124.
Sundberg, F.A., Karlstrom, K.E., Geyer, G., Foster, J.R., Hagadorn, J.W., Mohr, M.T., Schmitz, M.D., Dehler, C.M., Crossey, L.J., 2020. Asynchronous trilobite extinctions at the early to middle Cambrian transition. Geology 48 (5), 441–445. https://doi.org/10.1130/G46913.1.
Sundberg, F.A., Webster, M., Geyer, G., 2022. Biostratigraphical significance of a new trilobite fauna from the Harkless Formation (upper stage 4, Series 2, Cambrian), Ne./ t6f6giü 4.
Thoral, M., 1948. Solenopleuridae et Liostracidae languedociens. Annales de l'Université de Lyon, section C, Sciences Naturelles 5, 1–89.
Torsvik, T.H., Cocks, L.R.M., 2013. Gondwana from top to base in space and time. Gondwana Res. 24 (3–4), 999–1030. https://doi.org/10.1016/j.gr.2013.06.012.
Torsvik, T.H., Cocks, L.R.M., 2016. Cambrian. In: Earth History and Palaeogeography. Cambrige University Press, Cambridge, pp. 85–100. https://doi.org/10.1017/9781316225523.006.
Veizer, J., Ala, D., Azmy, K., Bruckschen, P., Buhl, D., Bruhn, F., Carden, G.A.F., Diener, A., Ebneth, S., Godderis, Y., Jasper, T., Korte, C., Pawellek, F., Podlaha, O.G., Strauss, H., 1999. $^{87}Sr/^{86}Sr$, $\delta^{13}C$ and $\delta^{18}O$ evolution of Phanerozoic seawater. Chem. Geol. 161 (1–3), 59–88. https://doi.org/10.1016/S0009-2541(99)00081-9.
Vizcaïno, D., Lefebvre, B., 1999. Les échinodermes du Paléozoïque inférieur de Montagne Noire : biostratigraphie et paléobiodiversité. Geobios 32 (2), 353–364. https://doi.org/10.1016/S0016-6995(99)80049-7.
Wang, X.L., Hu, W.X., Yao, S.P., Chen, Q., Xie, X.M., 2011. Carbon and strontium isotopes and global correlation of Cambrian Series 2-Series 3 carbonate rocks in the Keping area of the northwestern Tarim Basin, NW China. Mar. Pet. Geol. 28 (5), 992–1002. https://doi.org/10.1016/j.marpetgeo.2011.01.006.
Wotte, T., Álvaro, J.J., Shields, G.A., Brown, B., Brasier, M.D., Veizer, J., 2007. C-, O- and Sr-isotope stratigraphy across the Lower-Middle Cambrian transition of the Cantabrian Zone (Spain) and the Montagne Noire (France) West Gondwana. Palaeogeogr. Palaeoclimatol. Palaeoecol. 256 (1–2), 47–70. https://doi.org/10.1016/j.palaeo.2007.09.002.
Wotte, T., Strauss, H., Sundberg, F.A., 2011. Carbon and Sulfur Isotopes from the Cambiran Series 2 - Cambrian Series 3 of Laurentia and Siberia. Mus. North. Ariz. Bull. 67, 43–63.
Wotte, T., Strauss, H., Fugmann, A., Garbe-Schönber, D., 2012. Paired delta S^{34} data from carbonate-associated sulfate and chromium-reducible sulfur across the traditional Lower-Middle Cambrian boundary of W-Gondwana. Geochim. Cosmochim. Acta 85, 228–253. https://doi.org/10.1016/j.gca.2012.02.013.
Wu, Y.S., Wang, W., Jiang, H.X., Cui, Y., Zhao, R., Huang, Z.B., Yang, Z.L., Chen, Y.Q., 2021. Evolution patterns of seawater carbon isotope composition during the Cambrian and their stratigraphic significance. Geol. J. 56 (1), 457–474. https://doi.org/10.1002/gj.3957.
Yang, X., Li, Z., Gao, B., Zhou, Y., 2021. The Cambrian Drumian carbon isotope excursion (DICE) in the Keping area of the northwestern Tarim Basin NW China. Palaeogeogr. Palaeoclimatol. Palaeoecol. 571. https://doi.org/10.1016/j.palaeo.2021.110385.
Zhang, J., Edwards, C.T., Diamond, C.W., Lyons, T.W., Zhang, Y., 2021. Marine oxygenation, deoxygenation, and life during the early Paleozoic: an overview. Palaeogeogr. Palaeoclimatol. Palaeoecol. 584. https://doi.org/10.1016/j.palaeo.2021.110715.
Zhang, P., Wang, Y., Zhang, X., Wei, Z., Wang, G., Zhang, T., Ma, H., Wei, J., He, W., Ma, X., Zhu, C., 2022. Carbon, oxygen and strontium isotopic and elemental characteristics of the Cambrian Longwangmiao Formation in South China: Paleoenvironmental significance and implications for carbon isotope excursions. Gondwana Res. 106, 174–190. https://doi.org/10.1016/j.gr.2022.01.008.
Zhao, Y.L., Yuan, J.L., Babcock, L.E., Guo, Q.J., Peng, J., Yin, L.M., Yang, X.L., Peng, S.-C., Wang, C.J., Gaines, R.R., Esteve, J., Tai, T.S., Yang, R.D., Wang, Y., Sun, H.J., Yang, Y.N., 2019. Global Standard Stratotype-Section and Point (GSSP) for the conterminous base of the Miaolingian Series and Wuliuan Stage (Cambrian) at Balang, Jianhe, Guizhou China. Episodes 42 (2), 165–184. https://doi.org/10.18814/epiiugs/2019/019013.
Zhu, M.-Y., Zhang, J.M., Li, G.X., Yang, A.H., 2004. Evolution of C isotopes in the Cambrian of China: implications for Cambrian subdivision and trilobite mass extinctions. Geobios 37 (2), 287–301. https://doi.org/10.1016/j.geobios.2003.06.001.
Zhu, M.-Y., Babcock, L.E., Peng, S.-C., 2006. Advances in Cambrian stratigraphy and paleontology: Integrating correlation techniques, paleobiology, taphonomy and paleoenvironmental reconstruction. Palaeoworld 15 (3–4), 217–222. https://doi.org/10.1016/j.palwor.2006.10.016.
Zuo, J., Zhu, X., Chen, Y., Zhai, W., 2023. Carbon Isotope from Shallow Marine System in North China: Implications for Stratigraphical Correlation and Sea-Level changes in Cambrian. J. Earth Sci. 34 (6), 1777–1792. https://doi.org/10.1007/s12583-021-1463-6.